Universidade do Porto

Faculdade de Engenharia

Air flow and thermal analysis of an electrical transformers' substation

João Pedro Gonçalves Ferreira

Thesis submitted in partial fulfilment
of the requirements for the degree of
Master in Mechanical Engineering.

July 2014

Abstract

In this work, a numerical model is built in order to study the air flow and air temperature distribution inside a transformers substation.

The RaNS method and the realizable $k-\varepsilon$ are used to model turbulence. The finite control volume method has been used to discretize the continuity, momentum and energy equations in steady state.

An evaluation of convergence has also been made.

From the analysis of the results, it was possible to conclude about the influence of the equipments installed inside the room on the air flow pattern. It was concluded that the *Transformer 1750 kVA* has the most significant role in this matter, and a more detailed analysis of its influence is performed.

The hottest region of the model is the top surface of the *Transformer 1750 kVA*, while the coldest are adjacent to the air inlets on the side wall and on the front and back doors. The average interior air temperature is 39 °C.

It was noticed that the air that is being released in *LV Boards* outlets is entering on its inlets again, which leads to a decrease of the efficiency of the heat transfer process inside the equipment.

Finally, it must be stated that this model is yet to be validated with experimental data.

Key words:

- Air flow,
- Computational fluid dynamics,
- Finite volume method,
- Numerical model,
- Power transformer,
- Thermal analysis,
- Transformer substation,
- Ventilation.

Resumo

Neste trabalho, um modelo numérico é construído de modo a estudar o fluxo do ar e a distribuição da temperatura no interior de uma subestação de transformadores.

A modelação da turbulência foi feita usando o método RaNS e o modelo *realizable* $k-\varepsilon$. As equações de continuidade, quantidade de movimento e de energia, em regime estacionário, foram discretizadas usando o método dos volumes de controlo finitos.

Uma avaliação de erros de convergência foi igualmente realizada.

A partir da análise dos resultados foi possível concluir sobre a influência dos equipamentos instalados na circulação de ar no interior da substação. Concluiu-se que o *Transformer 1750 kVA* tem o papel mais importante nesta matéria, e realizou-se uma análise mais detalhada da sua influência.

A região com temperaturas mais elevadas é a superfície superior do *Transformer 1750 kVA*, enquanto que as mais baixas registam-se nas regiões adjacentes às entradas de ar na parede lateral e nas portas da frente e trás. A temperatura média do ar interior é de 39 °C.

Observou-se que o ar que está a ser ventilado nas saídas dos *LV Boards* está a entrar novamente pelas suas grelhas, o que leva a uma diminuição da eficiência do processo de transferência de calor no interior do equipamento.

Finalmente, há que referir que este modelo ainda não se encontra validado por dados experimentais.

Palavras-chave:

- Circulação de ar,
- Método dos volumes de controlo finitos,
- Transformador de potência,
- Subestação de transformação,
- Mecânica de fluidos computacional,
- Modelo numérico,
- Análise térmica,
- Ventilação.

Resumen

En este trabajo, un modelo numérico se construyó con el fin de estudiar el flujo de aire y distribución de la temperatura del aire dentro de una subestación de transformadores.

El método RaNS y *realizable* $k-\varepsilon$ se utilizan para modelar la turbulencia. El método de los volúmenes de control finitos se ha utilizado para resolver las ecuaciones de continuidad, cantidad de movimiento y energía en estado estacionario.

También se ha hecho una evaluación de los errores de convergencia.

A partir del análisis de los resultados se puede concluir sobre la influencia de los equipos instalados en la circulación del aire dentro de la subestación. Se concluyó que lo *Transformer 1750 kVA* tiene el papel más importante en esto, y nos llevó a cabo un análisis más detallada de su influencia.

La región más calurosa del modelo es la superficie superior de la *Transformer 1750 kVA*, mientras que las más frías son adyacentes a las entradas de aire en la pared lateral y en las puertas delanteras y traseras. La temperatura del aire interior media es de 39 °C.

Se dio cuenta de que el aire que está siendo lanzado en los puntos de venta de los *LV Boards* está entrando en sus entradas de nuevo, lo que conduce a una disminución de la eficiencia del proceso de transferencia de calor en el interior del equipo.

Por último, hay que señalar que este modelo aún no se ha validado con datos experimentales.

Palabras clave

- Circulacion de l'aire,
- Método de los volúmenes, de control finitos
- Transformador de potencia,
- Subestación transformadora,
- Dinámica de fluidos computacional,
- Modelo numérico,
- Análisis térmica,
- Ventilación.

Acknowledgements

On the verge of finishing this thesis, I would like to express my gratitude to everyone that have helped me throughout my entire academic path.

First of all, I would like to thank my supervisor, Prof. Laginha Palma, for all the support given throughout this work. He has been a great professional example for me, and has taught me so much more than fluid mechanics. His humour has also been a pleasant surprise. I thank him for what has been a truly experience of a lifetime, since the very day of the famous meeting with one Spanish gentleman.

I also thank Prof. Alexandre Silva Lopes, who taught me who is the *'Cristiano Ronaldo'* of fluid mechanics; Prof. Carlos Veiga Rodrigues, my former Fluid Mechanics teacher, and Vitor Gomes, who shared its 29^{th} birthday *bolas de berlim* with me. They gave me a truly **warm** welcome in their 4th floor loft, and presented me with good advises and good companionship.

I thank Prof. Teresa Duarte, who, perhaps without knowing, have helped me so much throughout this years, since the very first day, on the *Física Química* course.

I would like to make a deserved unnamed mention to all my former professors that have somehow inspired me.

I cannot forget to thank my colleagues and friends, whose friendship and patience has been of the most importance to me. I will surely miss all the classes we have gone and skipped together. I also have to thank Márcio for letting me join his *Sistemas de Controlo* group.

And finally, I cannot ever thank my family what they have been doing for me for the past 23 years. I hope someday to deserve all the sacrifices they have made for me, and I intend to pay them everyday with love.

JOÃO FERREIRA

"O mundo é para quem nasce para o conquistar
e não para quem sonha que pode conquistá-lo,
ainda que tenha razão."

Álvaro de Campos

Contents

List of Figures

List of Tables

Nomenclature

Abbreviations

AC	Alternating current.
CAD	Computer assisted design.
CFD	Computational fluid dynamics.
CPU	Central processing unit.
DC	Direct current.
DNS	Direct numerical simulation.
GCI	Grid convergence index.
LES	Large eddy simulation.
LV	Low voltage.
MV	Medium voltage.
PISO	Pressure-implicit with splitting of operators.
QUICK	Quadratic upwind interpolation scheme.
RAM	Random access memory.
RaNS	Reynolds averaged Navier-Stokes.
SIMPLE	Semi-implicit method for pressure-linked equations.

SIMPLEC	Semi-implicit method for pressure-linked equations (consistent).
SIMPLER	Semi-implicit method for pressure-linked equation (revised).

Greek symbols

α_{21}, α_{32}	Absolute differences.
ΔA	Difference of two values of quantity A.
ε	Turbulence energy dissipation.
ϕ	Generic quantity.
η	Variable used in realizable $k-\varepsilon$ model.
μ	Dynamic viscosity.
μ_t	Turbulent dynamic viscosity.
ν	Kinematic viscosity.
ρ	Density.
σ_ε	Turbulent Prandtl number for ε.
σ_k	Turbulent Prandtl number for k.
σ_Θ	Turbulent Prandtl number for energy.
$\overline{\overline{\tau}}$	Deviatoric stess tensor.
ω_k	Angular velocity.

Γ	Diffusivity coefficient.
Y_j	Mass fraction of species j.
Ω	Volume of bounded region of space.
$\overline{\Omega}_{ij}$	Mean rate-of-rotation tensor viewed in a moving reference frame.

Roman symbols

A_0, A_S	Variables used in realizable $k-\varepsilon$ model.
$\vec{A}_f$	Surface area vector of face f.
a_P	Center coefficient of the cell.
a_{nb}	Influence coefficient of neighbouring cells.
$C_1, C_\mu, C_{\varepsilon 1}, C_{\varepsilon 2}$	Constants used in standard and realizable $k-\varepsilon$ model.
c_0, c_1	Centroids of cells 0 and 1.
c_p	Isobaric specific heat.
d_f	Variable used in the discretization of the continuity equation.
E	Total energy.
$\vec{F}$	Sum of external body forces.
F, F_k	Control volume surface (k) .

F_S	Factor of safety.
$\vec{g}$	Acceleration due to gravity.
G_b	Rate of production of turbulent kinetic energy by buoyancy.
G_k	Rate of production of turbulent kinetic energy by the mean flow.
h	Sensible enthalpy.
I	Identity matrix.
$\vec{J}$	Diffusion flux.
$\vec{J}_f$	Mass flux through face f.
k	Turbulent kinetic energy.
k_{eff}	Effective conductivity.
m	Mass.
$\vec{n}$	Normal direction vector to surface S.
p	Pressure; order of convergence.
p_{c0}, p_{c1}	Pressure on the cell centroids 0 and 1.
Q	Energy transferred under the form of heat.
$Q_{\phi,P}$	Total value of a quantity ϕ on the cell center.
q_ϕ	Source of a certain quantity ϕ in the interior of the volume element.
$\vec{r}_0, \vec{r}_1, \vec{r}$	Displacement vector from the upstream cell centroid to the face centroid.
S_{ij}	Rate of strain.

S, S_k	Surface (k).
S_x, S_y, S_z	Source terms in the equations.
t	Time.
T	Temperature.
$\vec{u}$	Velocity vector.
$u_{n,c0}, u_{n,c1}$	Normal velocity on the centroids of cells 0 and 1.
U^*	Variable used in realizable $k-\varepsilon$ model.
v	Velocity.
V	Volume.
$\dot{V}$	Volume flow rate.
W	Energy transferred under the form of work.
W	Variable used in realizable $k-\varepsilon$ model.

Subscripts and superscripts

i, j, k	Referent to the standard basis vectors of the Cartesian coordinate system.
x, y, z	Referent to a Cartesian direction.
u, v, w	Referent to a component of the velocity vector.
P, N	Referent to the center of the control volume.
S, f	Referent to a control volume surface.

Operators and mathematical symbols

$\left\{\vec{i},\vec{j},\vec{k}\right\}$	Standard basis vectors for the Cartesian coordinate system.
δ_{ij}	Kronecker delta.
ε_{ijk}	Levi-Civita symbol.
$\partial A/\partial B$	Partial derivative of variable A in order to B.
$\partial^2 A/\partial B^2$	Second derivative of variable A in order to B.
$\partial^2 A/\partial B\partial C$	Second order mixed derivatives of variable A in order to B and C.
$\max\left[A,B\right]$	Maximum value of the set.
∇A	Gradient operator.
$\nabla\cdot\vec{A}$	Divergence of vector $\vec{A}$.
$\dot{A}$	Rate of change of quantity A with time.
$\overline{A}$	Time average of quantity A.
$\overline{\overline{A}}$	Matrix, second rank tensor.
A'	Turbulent fluctuation of quantity A.
$\vec{A}^T$	Transpose of matrix $\vec{A}$.

Chapter 1

Introduction

1.1 Motivation

The knowledge and comprehension of fluid flow and heat transfer phenomena are of the most importance in mechanical engineering applications. There were always two different ways to approach and solve these kind of problems: experimental investigation and theoretical study.

The most reliable information about physical phenomena is obtained through experimental investigation. However, this method presents itself some limitations. In some cases, real scale models are too expensive or even impossible to reproduce. And even scale models measurements may not be extrapolated to the real case. Plus, all measures are affected by systematic and random errors (Patankar, 1980; Ferziger and Perić, 2002).

Theoretical study consists in solving the mathematical model of the system considered. In mechanical engineering applications, these mathematical models usually consist in a set of differential equations (*e.g.* Navier-Stokes equations). However, using the classical mathematical solving methods, it is only possible to solve this equations for a few, simple cases and mostly with reduced practical application.

One third and more recent approach to solve this kind of problems consists in computational calculation analysis. Considering the evolution on digital computation, it is possible to solve the mathematical model differential equations, making the computer modelling more powerful and widely applicable (Patankar, 1980).

Computer simulation of fluid flow, also known as Computational Fluid Dynamics (CFD), has allowed scientists and engineers to see the complexities in flow physics and

errors arising from theoretical models. But it is also a powerful tool for solving a wide variety of industrial problems with prompt turnaround time (Ferziger and Perić, 2002).

From the point of view of conception and project, the possibility of designing one product for some desired performance, and continuously optimize it even before start producing it, makes CFD a fast, low cost and very attractive tool. Industries like aerospace, automotive, power generation, chemical manufacturing, polymer processing, petroleum exploration, medical research, meteorology, internal combustion engines and turbo machinery, are some of the many who have been using CFD to research and develop their projects.

The knowledge and understanding of these CFD concepts can be of great utility for the formation of a mechanical engineer, hence the interest in this particular field of study.

There are some natural advantages of numerical calculation. First, the low cost of the computational simulation compared with experimental investigation. Second, the speed of the process, since a computer run is faster than an experimental proceeding. Third, the quality of the information, since the computational solution provides values of all relevant variables within the domain of the problem (flow field, pressure field, temperature distribution). And finally, the possibility to simulate ideal case conditions and real case conditions (Patankar, 1980).

Nevertheless, there are still some limitations in this kind of analysis. In some studies of turbulent flows or some non-Newtonian fluid flows, there are not yet accurate mathematical models that describe this phenomena, thus the results of numerical simulations will not be accurate as well. In the same way, in some studies of very complex geometries, high non-linearity or strong sensitive variation of fluid properties, it can be very difficult to obtain a numerical solution.

Numerical simulation *per se* is not sufficient, as it is needed to proceed to a verification and validation of the results. The verification is done to ensure that there are no numerical errors and the code produces the same results with different mesh. The validation of the results is performed by comparing the results obtained in the numerical simulation with experimental results or another numerical simulation results already validated (Roache, 1998).

So it is plausible to assume that numerical analysis should (and must) always be complemented with experimental investigation.

1.2 Case study description

The work developed on this thesis is based on a multi-national project denominated *Aura Solar*, that involves the cooperation of solar power exploration and electrical transformation specialized companies from Portugal, Spain and Mexico.

The *Aura Solar* project comprises the construction and operation of a 40 MW greenfield photovoltaic power plant on an area of 100 ha located 10 km from La Paz, Baja California Sur, Mexico.[1]

It is expected to generate 82 GWh per year from the 131800 photovoltaic modules installed, enough to supply the electrical power needs of 164000 inhabitants. It is the biggest solar plant in Latin America, and represents an investment 100 Million U.S. dollars. [1]

Figure 1.1: The *Aura Solar* solar power plant.[1]

Electricity is generated in the solar power plant, and is then supplied to a transformer substation near the photovoltaic modules. In the transformer substation, the voltage is increased substantially using step up transformers. The voltage is increased to reduce the transmission losses over long distances. In this case, the substation is installed inside a container, as it is presented on Figure 1.2.

As it is possible to observe on Figure 1.2, the substation container is divided into two different rooms. The *Inverters' room*, on the left, is where the inverters are located. They are responsible for changing the Direct Current (DC) into Alternating Current (AC). The *Transformers' room*, on the right, is where the equipments for the transformation of the electric power are installed.

[1] http://www.aurasolar.com.mx/index.html, accessed in 20-05-2014

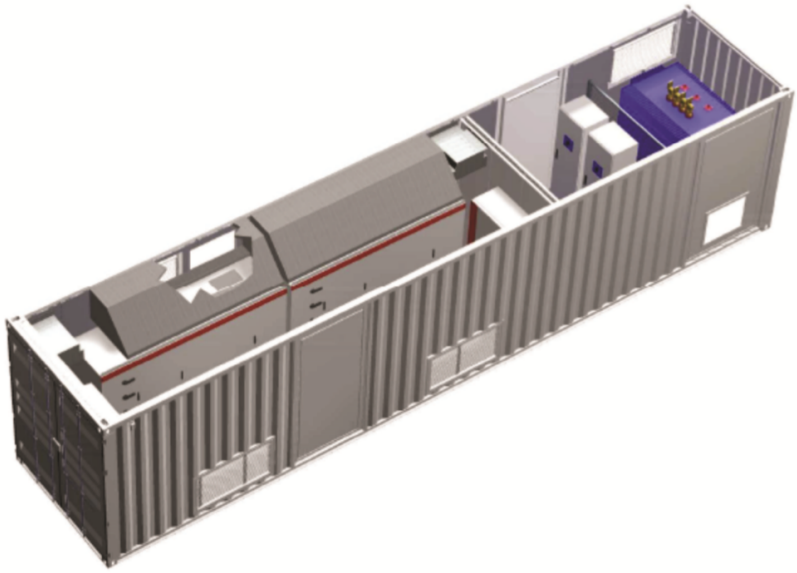

Figure 1.2: Substation container of the *Aura Solar* power plant.

In this work, the main subject of analysis will be the *Transformers' room*. A full description of this room is presented in the next section.

1.2.1 The *Transformers' room*

The interior of the *Transformers' room* can be seen in Figure 1.3. The main dimensions are 4.3 m $\times$ 2.4 m $\times$ 2.9 m , in length, width and height, respectively. The ventilation of the room is guaranteed by four air inlets and one ventilator.

There are two inlets installed in the exterior side wall, and one in each door (front and back). The ventilator is installed on the back wall. It is expected to ventilate a flow rate of 5500 m^3/h.

There are five distinct equipments installed inside the room (Figure 1.3). They are presented and described in the next lines.

Transformer 1750 kVA and *Transformer 50 kVA*

The main equipments installed inside are two different power transformers, with rated powers of 1750 and 50 kVA. They are installed next to the side walls of the container.

A power transformer is a device that employs the principle of mutual induction to convert variations of alternating current in a primary circuit into variations of electrical

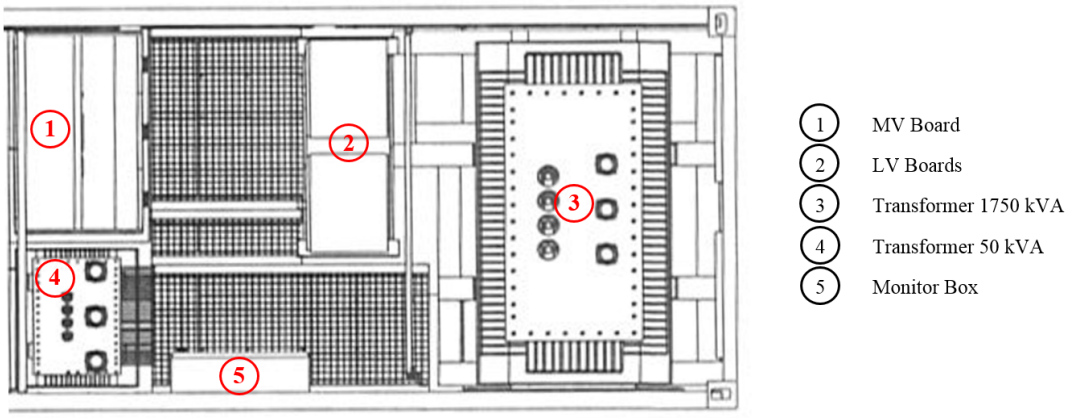

Figure 1.3: Legended blueprint of the interior of substation container of the *Aura Solar* power plant.

parameters like voltage and current in a secondary circuit at the same frequency (El Wakil et al., 2006). In the present case, the two of them are used to raise the voltage of the electricity generated at the power plant to the high levels used to transmit the electricity into the net distribution.

The efficiency of a transformer is influenced by the heat losses occurring in the different circuits, due firstly to the variation of the alternate magnetic flux in the iron and secondly to the Joule effect and Foucault currents which produce an undesirable heat (Tsili et al., 2012). Therefore, from an economical and safety point of view, it is necessary to cool the transformer in order to preserve it.

LV Boards

The Low Voltage boards consist in a modular structure of two different blocks, and their function is to receive the main Low Voltage circuit coming from the transformers and distribute it to a given number of individual circuits.

This equipment has its own internal ventilation system, expected to ventilate a flow rate of 1400 m^3/h. Therefore, it presents two air inlets and ventilators on each door, and two additional ventilators on the top.

MV Board and *Monitor Box*

The Medium Voltage (MV) Board is installed next to the *Inverters' room* side wall, on the right side of the back door entrance. The *Monitor Box* is placed on the front wall, right

in front of the back door. Both present no considerable heat generation rate, and, in this work, their presence is expected to influence only the air flow pattern inside the room.

AC cables

The AC cables are located below the technical floor. The technical floor is a metallic grid that is placed on the floor of the container, right above the cables that are connecting the transformers to the inverters on the contiguous room. In order to model these cables, some simplifications will have to be made, since there is no knowledge about their precise location on the floor.

1.2.1.1 Heat sources

There are equipments inside the *Transformers' room* that generate heat. Usually, this heat is removed by natural convection of air flowing through the substation, crossing the grids placed on the walls (Ramos et al., 2013).

In addiction, there is also heat transferred by radiation between the equipments and the walls.

The heat released by the installed equipments was quantified and presented in a previous study, performed by one of the business partners of the project. All heat fluxes used on the numerical model are based on this study.

Table 1.1 presents the study values of the heat generation in each equipment.

These values refer to a situation where all the equipments are working at full load, which corresponds to the situation where the heat generation is the highest. This scenario is not supposed to happen often in the reality, but will be taken in consideration in this work, in order to simulate a critical situation.

The values of the heat flux on the walls and roof are due to insulation effects. In order to model these effects more accurately, it should be considered input an heat flux value dependent on the time of the day. This proposal is revised in § 3.6.6.

The heat flux on the floor is an approximation of the effects of the AC cables that connect the transformers and the inverters. They are located on the ground, hence this simplification.

Table 1.1: Heat generation of each equipment inside the *Transformers' room*.

	Heat generation rate $[W]$
Transformer 1750 kVA	20900.00
Transformer 50 kVA	1290.00
LV Boards	1700.00
Front wall	326.55
Back wall	326.55
Inverters' room side wall	-110.25
Exterior side wall	183.75
Roof	326.55
Floor	1503.07
Total:	26446.22

The negative heat flux on the *Inverters' room* side wall is related to the thermal gradient between the two rooms, and corresponds to a loss of heat rather than a gain. It is properly described also on § 3.6.6.

1.3 Objectives

This work is meant to be an application of CFD concepts on the solution of mechanical engineering problems.

The purpose of this thesis is to elaborate a complete air flow and thermal study of the *Transformers' room* described in § 1.2. This study must be an accurate approximation of the real case scenario. At first, it was important to understand the constitution and functioning of each element present inside the room.

In order to perform this study, a numerical model was created. A CAD geometry was built combining the analysis of blueprints and measures taken on site. From this geometry,

a computational mesh was generated and introduced in a computational software that numerically solved the equations in this domain (ANSYS® *Fluent*).

With a full defined numerical model, it was possible to reproduce the real pattern of air circulation inside the container and calculate the volume flow rates on the inlets and outlets. It was also possible to input the heat flux transferred to the air and quantify the spacial distribution of the temperature of the air and surface temperature of the equipments and walls.

In the end, it was performed an analysis of the air flow and temperature distribution profiles inside the *Transformers' room*, as well as a detailed analysis of the influence of the most important elements on these processes.

1.4 Brief introduction to the CFD software

The CFD analysis of the case study was performed with the commercial software ANSYS® *Workbench*. It is one of the most used CFD codes in the world, and it is used by a wide variety of industries.

ANSYS® *Workbench* is a computational platform that joins together the entire simulation process in the same framework, and allows the user to work separately on the different stages. The features of the program include a CAD software for building geometries (ANSYS® *Design Modeller*), a mesh generator (ANSYS® *Meshing*), the software used to perform the fluid flow analysis (ANSYS® *Fluent*) and also a program to post-process the results (ANSYS® *CFD-Post*).

The program main advantages are simplicity of use and the possibility to load geometry files built with other CAD softwares, like SolidWorks®. It also presents the possibility of performing multi-physics analysis of the same problem.

1.5 Outline of the thesis

This thesis is divided in four chapters, including the present *Introduction*. In this chapter there are a complete, detailed description of the case study, a brief introduction to the software used to perform the numerical simulation and the main objectives of this work.

In Chapter 2 it is presented the mathematical model of the case, and the mathematical description of all fundamental equations and turbulence models. In this chapter there is

also an overview of the techniques used to numerically solve the model, with mention to the use of finite volume method for the discretization of the governing equations, and the solver algorithm.

The construction of the computational model of the *Transformers' room* is presented in Chapter 3. A complete report on the definition of the geometry, the generation of the computational mesh, boundary conditions and material properties is made. The simulation results are presented in the end of the chapter.

Finally, Chapter 4 summarizes the main conclusions of the thesis. In the end, there are also some suggestions of additional studies based on this work.

Chapter 2

Mathematical model and numerical techniques

Abstract

In this chapter, the fundamental equations of the mathematical model are presented. These equations express the principles of conservation of mass, momentum and energy. The Reynolds averaged Navier-Stokes method and the two turbulence models, k-ε and realizable k-ε, are here described, so as the numerical techniques used to solve the equations, involving a finite volume discretization method and the solver algorithm. The contents of the chapter were based on previous works of Silva Lopes (2000) *and* Veiga Rodrigues (2013).

2.1 Mathematical model

2.1.1 Fundamental equations

The starting point of any numerical simulation is the mathematical model. The model here described is based on the continuity, momentum and energy conservation equations in differential form. In the next sections these fundamental equations are presented, as well as some of the simplifications considered. All equations and vectors are expressed in Cartesian coordinate system.

2.1.1.1 Continuity equation

Following Batchelor (1967), the principle of conservation of mass applied to an infinitesimal portion of fluid volume can be described by Eq. (2.1):

$$\frac{\partial \rho}{\partial t} + \nabla \cdot (\rho \vec{u}) = 0, \tag{2.1}$$

where ρ is the fluid density, t is time and $\vec{u}$ is the velocity vector. Considering the case of a steady state, incompressible flow, the continuity equation can be simplified to Eq. (2.2):

$$\nabla \cdot (\vec{u}) = 0 \tag{2.2}$$

2.1.1.2 Momentum transport equation

The equations of conservation of momentum arise from the application of Newton's second law to an infinitesimal portion of fluid in motion. These equations represent a relation between velocity field (or flow field) and pressure field, and they comprehend the values of velocity and pressure of the fluid at a given point in space and time. According to Batchelor (1967), these equations can be written as Eq. (2.3):

$$\frac{\partial}{\partial t}(\rho \vec{u}) + \nabla \cdot (\rho \vec{u}\vec{u}) = -\nabla p + \nabla \cdot \left(\overline{\overline{\tau}}\right) + \rho \vec{g} + \vec{F}, \tag{2.3}$$

where p is the static pressure, $\rho \vec{g}$ is the gravitational body force and $\vec{F}$ represents the sum of all external body forces. Considering that the fluid is Newtonian, *i.e.*, viscous stress is proportional to the local strain rate, the stress tensor $\overline{\overline{\tau}}$ is defined by Batchelor (1967) as:

$$\overline{\overline{\tau}} = \mu \left[\left(\nabla \vec{u} + \nabla \vec{u}^T \right) - \frac{2}{3} \nabla \cdot \vec{u} I \right], \tag{2.4}$$

where μ is the dynamic viscosity of the fluid and I is the identity matrix. Although the dynamic viscosity depends significantly on the temperature, it is considered that there are no appreciable differences on the temperature of the fluid. Therefore, μ is taken as uniform all over the fluid.

These three equations of conservation of momentum (one for each component of the velocity vector) are known as Navier-Stokes equations.

2.1.1.3 Energy transport equation

The principle of conservation of energy can be properly described by the first law of thermodynamics. According to Munson et al. (2009), it states that the time rate of increase of the total stored energy in a system, E, is equal to the sum of the net time rate of energy addiction by heat transfer and work into the system. This principle is expressed in Eq. (2.5):

$$\frac{dE}{dt} = \partial\dot{Q} + \partial\dot{W}, \tag{2.5}$$

where

$$E = m\left(h - \frac{p}{\rho} + \frac{\vec{u}\cdot\vec{u}}{2}\right). \tag{2.6}$$

For details about the deduction of the energy equation, please refer to §5.3 in Munson et al. (2009) and §2.1.4 in Versteeg and Malalasekera (2007).

The representation of the steady state energy equation used in this work is presented in Eq. (2.7), and it is adapted from ANSYS Documentation (2013):

$$\nabla\cdot\left(\rho\vec{u}\left(h + \frac{\vec{u}\cdot\vec{u}}{2}\right)\right) = \nabla\cdot\left(k_{eff}\nabla T - h\vec{J} + \left(\overline{\overline{\tau}}\cdot\vec{u}\right)\right). \tag{2.7}$$

The first term of the right hand side of the equation represent energy transferred due to conduction, where k_{eff} is the effective conductivity and results from the sum of the conductivity of the fluid k with the turbulent thermal conductivity k_t, defined according to the turbulence model used. The second term represents the energy transferred due to species diffusion, where h is the sensible enthalpy and $\vec{J}$ is the diffusion flux. The third term represents the energy lost due to viscous dissipation.

2.1.2 Turbulence models

There are several possible ways to solve the governing solutions. Considering a case with very simple flow and geometry, it is possible to obtain an analytical solution.

Another way consists in numerically solve the governing equations, proceeding only to the needed discretization of the equations. This method, named *Direct Numerical Simulation* (DNS), is reviewed in Moin and Mahesh (1998). In DNS, the Navier-Stokes equa-

tions are numerically solved without any turbulence model. All scales of turbulence are computed, from the integral scale to the dissipative scale, which requires a large number of grid points (Choi and Moin, 2012). As consequence, there are significant costs regarding computer processing and memory storage, making these unfeasible for engineering applications.

In order to reduce the time and computational resources and obtain relevant solutions, alternative methods need to be considered for modelling turbulence. Two of these methods are Reynolds averaged Navier-Stokes (RaNS) and Large Eddy Simulation (LES).

RaNS method was proposed by Reynolds (1895), and states that an instantaneous flow variable quantity can be decomposed into an ensemble-averaged term and a turbulent fluctuating term. This method is reviewed in Speziale (1991).

LES was first proposed by Smagorinsky (1963), and consists in directly compute the large energy-containing scales (integral scales), while modelling the influence of the small scales rather than resolving them. The theory and application of LES can be found in Lesieur and Métais (1996) and Moin (1997).

In this work, the approach used for turbulence modelling is the RaNS method.

2.1.2.1 Steady Reynolds averaged Navier-Stokes equation

The Reynolds averaged Navier-Stokes method (Reynolds, 1895) is based on Reynolds decomposition. It states that in a statistically steady flow, every variable can be decomposed as the sum of a time averaged value and a fluctuation about that value (Ferziger and Perić, 2002):

$$\phi\left(x_i,t\right) = \overline{\phi}\left(x_i\right) + \phi'\left(x_i,t\right), \tag{2.8}$$

where $\overline{\phi}$ represents the mean component and ϕ' the fluctuation component. It can also be stated that:

$$\overline{\overline{\phi}} \equiv \overline{\phi}, \tag{2.9}$$

$$\overline{\phi'} = 0, \tag{2.10}$$

and $\overline{\phi}(x_i)$ can be defined as:

$$\overline{\phi}(x_i) = \lim_{T\to\infty} \frac{1}{T} \int_0^T \phi(x_i,t)\, dt \tag{2.11}$$

In Eq. (2.11), t is the time and T stands for the averaging interval. This interval must be large enough so that $\overline{\phi}$ does not depend on the time at which the averaging is started.

The continuity and Navier-Stokes equations in steady state, after Reynolds decomposition and averaging, become:

$$\frac{\partial}{\partial x_i}(\rho \overline{u}_i) = 0, \tag{2.12}$$

$$\frac{\partial}{\partial x_j}(\rho \overline{u}_i \overline{u}_j) = -\frac{\partial p}{\partial x_i} + \frac{\partial}{\partial x_j}\left[\mu\left(\frac{\partial \overline{u}_i}{\partial x_j} + \frac{\partial \overline{u}_j}{\partial x_i} - \frac{2}{3}\delta_{ij}\frac{\partial \overline{u}_l}{\partial x_l}\right)\right] + \frac{\partial}{\partial x_j}\left(-\rho\overline{u_i' u_j'}\right), \tag{2.13}$$

where δ_{ij} is the Kronecker delta.

These equations have the same general form as the instantaneous (exact) Navier-Stokes equations, with the velocities and other solution variables now representing time-averaged values. Additional terms now appear that represent the effects of turbulence. These Reynolds stresses, $-\rho\overline{u_i' u_j'}$, must be modelled in order to close Eq. (2.13).

In order to properly model the Reynolds stress tensor, two turbulence models were considered: the k-ε model and the realizable k-ε model, which is an extension to the first. Due to the complexity of the turbulence phenomena, it is not expected that one single turbulence model can lead to relevant results in all kinds of flows (Kline et al., 1980). Therefore, other turbulence models can be found in Launder and Spalding (1972) or Launder et al. (1975).

2.1.2.2 The k-ε turbulence model

The k-ε turbulence model was first proposed by Launder and Spalding (1972). It has the largest range of applicability, and presents accurate results in simple flow cases (Pope, 2000). It is considered as a semi-empirical model, and the derivation of the model equations relies on phenomenological considerations and empiricism (ANSYS Documentation, 2013).

The low computational effort required makes this model one of the most used for the

solution of practical engineering problems (Speziale, 1991). Therefore, it is incorporated in most of CFD commercial softwares.

The k-ε model consists of two model transport equations, for turbulent kinetic energy, k, and its dissipation rate, ε, and the specification of the turbulent viscosity μ_t.

The eddy viscosity is expressed as:

$$\mu_t = \rho C_\mu \frac{k^2}{\varepsilon}, \tag{2.14}$$

where C_μ is a constant parameter that will be defined later on this section.

Following Ferziger and Perić (2002), the eddy-viscosity model for the Reynolds stress is given in Eq. (2.15):

$$-\rho\overline{u_i' u_j'} = \mu_t \left(\frac{\partial \overline{u}_i}{\partial x_j} + \frac{\partial \overline{u}_j}{\partial x_i} \right) - \frac{2}{3}\rho \delta_{ij} k \tag{2.15}$$

The turbulent kinetic energy k is:

$$k = \frac{1}{2}\overline{u_i' u_i'} = \frac{1}{2}\left(\overline{u_x' u_x'} + \overline{u_y' u_y'} + \overline{u_z' u_z'}\right) \tag{2.16}$$

A transport equation for turbulent kinetic energy can be derived from the steady RaNS equations:

$$\frac{\partial}{\partial x_i}\left(\rho \overline{u}_j k\right) = \frac{\partial}{\partial x_j}\left[\left(\mu + \frac{\mu_t}{\sigma_k}\right)\frac{\partial k}{\partial x_j}\right] + G_k + G_b - \rho\varepsilon, \tag{2.17}$$

where σ_k is the turbulent Prandtl number. The term G_k is the rate of production of turbulent kinetic energy by the mean flow, and it is expressed in Eq. (2.18). The term G_b is the rate of production of kinetic energy by buoyancy (when a non-zero gravity field and temperature gradient are present simultaneously), and it is expressed in Eq. (2.19).

$$G_k = -\rho\overline{u_i' u_j'}\frac{\partial u_j}{\partial x_i}, \tag{2.18}$$

$$G_b = -g_i \frac{\mu_t}{\rho \sigma_\Theta}\frac{\partial \rho}{\partial x_i}, \tag{2.19}$$

where g_i is the component of the gravitational vector on the direction i and σ_Θ is the Prandtl turbulent number for energy, and his default value is 0.85.

Unlike the transport equation for turbulent kinetic energy, the standard model equation for ε is rather empirical (Pope, 2000). According to Ferziger and Perić (2002), the most commonly form is:

$$\frac{\partial}{\partial x_i}(\rho\varepsilon\overline{u}_i) = \frac{\partial}{\partial x_j}\left[\left(\mu + \frac{\mu_t}{\sigma_\varepsilon}\right)\frac{\partial\varepsilon}{\partial x_j}\right] + C_{\varepsilon 1}\frac{\varepsilon}{k}G_k - C_{\varepsilon 2}\rho\frac{\varepsilon^2}{k}. \tag{2.20}$$

In Eq. (2.20), the terms $C_{\varepsilon 1}$ and $C_{\varepsilon 2}$ are constants, and the term σ_ε is the Prandtl turbulent number for ε.

The standard values of the model constants where proposed by Launder and Sharma (1974) and have been determined from experiments. They are presented on Table 2.1:

Table 2.1: Constants used in the k-ε model

$C_{\varepsilon 1}$	$C_{\varepsilon 2}$	C_μ	σ_k	σ_Θ	σ_ε
1.44	1.92	0.09	1.00	0.85	1.30

A variant of this turbulence model was considered, and it is described in the following section.

2.1.2.3 The realizable k-ε turbulence model

The realizable k-ε model was first proposed by Shih et al. (1995). The term "realizable" means that the model satisfies certain mathematical constraints on the Reynolds stresses, consistent with the physics of turbulent flows (ANSYS Documentation, 2013).

The main differences between the standard and the realizable models are the alternative formulation for the turbulent viscosity, μ_t, and a modified transport equation for the dissipation rate, that has been derived from an exact equation for the transport of the mean-square vorticity fluctuation (ANSYS Documentation, 2013).

Although the standard model performs quite well for boundary layer flows, the same does not happen for flows with a high mean shear rate or a massive separation, because in these cases the eddy viscosity is overpredicted by the standard eddy viscosity formulation. In addition, the standard model dissipation rate equation does not always give the appropriate length scale for turbulence (Shih et al., 1995).

The realizable k-ε model has been extensively validated for a wide range of flows, and its performance has been found to be substantially better than that of the standard k-ε model (Kim et al., 1997).

Like the standard k-ε model, the eddy viscosity is given from Eq. (2.15). The difference is that the term C_μ is no longer a constant, and it is given by:

$$C_\mu = \frac{1}{A_0 + A_S \frac{kU^*}{\varepsilon}}, \tag{2.21}$$

where

$$A_0 = 4,04, \tag{2.22}$$

$$A_S = \sqrt{6}\cos(\phi), \tag{2.23}$$

and

$$U^* \equiv \sqrt{S_{ij}S_{ij} + \tilde{\Omega}_{ij}\tilde{\Omega}_{ij}}. \tag{2.24}$$

The value of ϕ is obtained with Eq. (2.25):

$$\phi = \frac{1}{3}\cos^{-1}\left(\sqrt{6}W\right), \tag{2.25}$$

with

$$W = \frac{S_{ij}S_{jk}S_{ki}}{\tilde{S}^3}, \tag{2.26}$$

and

$$S_{ij} = \frac{1}{2}\left(\frac{\partial \overline{u}_j}{\partial x_i} + \frac{\partial \overline{u}_i}{\partial x_j}\right) \tag{2.27}$$

The values of $\tilde{\Omega}_{ij}$ and Ω_{ij} are computed from Eq. (2.28) and Eq. (2.29), and $\overline{\Omega}_{ij}$ is the mean rate-of-rotation tensor viewed in a moving reference frame with the angular velocity ω_k.

$$\tilde{\Omega}_{ij} = \Omega_{ij} - 2\varepsilon_{ijk}\omega_k, \tag{2.28}$$

$$\Omega_{ij} = \overline{\Omega}_{ij} - \varepsilon_{ijk}\omega_k. \tag{2.29}$$

In the realizable k-ε model, the transport equations for turbulent kinetic energy k and dissipation rate ε are:

$$\frac{\partial}{\partial x_j}\left(\rho\overline{u}_j k\right) = \frac{\partial}{\partial x_j}\left[\left(\mu + \frac{\mu_t}{\sigma_k}\right)\frac{\partial k}{\partial x_j}\right] + G_k + G_b - \rho\varepsilon, \tag{2.30}$$

and

$$\frac{\partial}{\partial x_i}\left(\rho\varepsilon\overline{u}_j\right) = \frac{\partial}{\partial x_j}\left[\left(\mu + \frac{\mu_t}{\sigma_\varepsilon}\right)\frac{\partial \varepsilon}{\partial x_j}\right] + \rho C_1 S\varepsilon - \rho C_{\varepsilon 2}\frac{\varepsilon^2}{k+\sqrt{\nu\varepsilon}}, \tag{2.31}$$

where ν stands for the kinematic viscosity. The value of C_1 is given by Eq. (2.32):

$$C_1 = \max\left[0{,}43, \frac{\eta}{\eta+5}\right], \tag{2.32}$$

with

$$\eta = S\frac{k}{\varepsilon}, \tag{2.33}$$

and

$$S = \sqrt{2S_{ij}S_{ij}}. \tag{2.34}$$

Note that the k equation is the same as that in the standard k-ε model, but the ε equation is rather different. One of the differences is that the production term in the ε equation (the second term on the right-hand side of Eq. 2.31) does not involve the production of k, *i.e.*, it does not contain the term G_k (ANSYS Documentation, 2013).

The model coefficients proposed by Shih et al. (1995) are summarized on Table 2.2:

Table 2.2: Constants used in the realizable k-ε model

C_1	$C_{\varepsilon 1}$	$C_{\varepsilon 2}$	C_μ	σ_k	σ_Θ	σ_ε
Eq. (2.32)	1.44	1.90	Eq. (2.21)	1.00	0.85	1.20

2.2 Numerical techniques

At the current state of knowledge, it is impossible to reach a solution for this kind of mathematical model without a using a numerical solving method. This part of the process is of great importance. If Navier-Stokes are solved accurately, it is possible to obtain a complete data set from which any quantity of physical significance can be derived (Ferziger and Perić, 2002).

The numerical solution implies a simplification of the governing equations used. The process begins with the division of the domain in discrete control volumes, using a computational grid. After this, the governing equations are integrated on these control volumes, in order to construct algebraic equations for the discrete dependent variables. The final steps are the linearization of the discretized equations and the solution of the resultant linear equation system (ANSYS Documentation, 2013).

2.2.1 Finite volume method

The most important approaches in CFD are finite difference, finite element and finite volume methods. Others, like spectral schemes, boundary element methods or cellular automata, have their use limited to specific problems (Ferziger and Perić, 2002). In theory, all of this methods should provide the same results if the grid is fine enough. In this work, finite volume method was considered.

As it is said before, the solution domain is divided in small control volumes by a computational grid. In Figure 2.1 it is represented an example of a finite control volume.

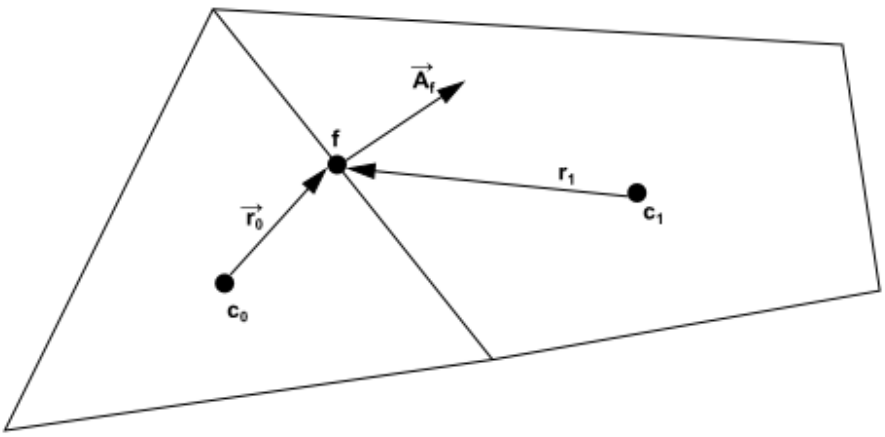

Figure 2.1: Control volume used to illustrate the discretization of a transport equation (ANSYS Documentation (2013)).

The coefficients c_0 and c_1 are the centroids of the cells *0* and *1*, $\vec{r}_0$ is the displacement vector from the upstream cell centroid to the face centroid, r_1 is the distance between the centroid c_1 and the face point *f*. Finally, $\vec{A}_f$ is the surface area vector of face *f*.

In problems where fluid flow plays a significant role, the effects of convection and diffusion have to be considered (Versteeg and Malalasekera, 2007). The steady state convection–diffusion equation can be derived from the transport equation, and serves as starting point for the analysis of each volume element. It represents the flux balance in a control volume (Ferziger and Perić, 2002):

$$\int_S (\rho\phi\vec{u}\cdot\vec{n})\,dS = \int_S (\Gamma\nabla\phi\cdot\vec{n})\,dS + \int_\Omega \left(q_\phi\right) d\Omega, \tag{2.35}$$

where $\vec{n}$ is the normal direction vector to the surface S, and Ω is the volume of the element considered. The term q_ϕ refers to a source of a certain quantity ϕ in the interior of the volume element.

To obtain an algebraic equation for a control volume, the surface and volume integrals need to be approximated. Following Ferziger and Perić (2002), the surface integral can be written as:

$$\int_S F\,dS = \sum_k \int_{S_k} F\,dS, \tag{2.36}$$

where F is the convective ($\rho\phi\vec{u}\cdot\vec{n}$) or diffusive ($\Gamma\nabla\phi\cdot\vec{n}$) flux vector in the direction normal to the control volume face k. It can be approximated by:

$$\int_{S_k} F\,dS = \overline{F}_k S_k \approx F_k S_k \tag{2.37}$$

In the same way, the volume integral can be written as:

$$Q_{\phi,P} = \int_\Omega \left(q_\phi\right) d\Omega \tag{2.38}$$

and can be approximated by:

$$\int_\Omega \left(q_\phi\right) d\Omega = \overline{q}_\phi \Delta\Omega \approx q_{\phi,P}\Delta\Omega, \tag{2.39}$$

where $Q_{\phi,P}$ is the total value of a quantity Q_ϕ and P is the denomination of the central node of the element. Therefore, $q_{\phi,P}$ stands for the value of q_ϕ at the center of the control volume element.

Higher-order approximations are referred in §4 in Ferziger and Perić (2002) and §3.2 in Patankar (1980).

2.2.1.1 Interpolation of a quantity ϕ

In spacial discretization, the discrete values of a quantity ϕ are, by default, computed at the center of volume elements. However, it is needed face values of ϕ to model the convection terms in Eq. (2.35). This face values have to be interpolated from the volume element center values (Ferziger and Perić, 2002).

This is accomplished using an upwind scheme. Upwinding means that the face value ϕ is derived from quantities in the cell upstream, or "upwind," relative to the direction of the normal velocity $\vec{u}$ in Eq. (2.35) (Versteeg and Malalasekera, 2007).

In the *first order upwind*, the quantities at the faces are determined by assuming that the center values of a certain quantity ϕ represent the volume element average value. Therefore, the face quantities are identical to the center quantities. Thus when first-order upwinding is selected, the face value ϕ_f is set equal to the center value of ϕ in the upstream cell (ANSYS Documentation, 2013).

When the flow is not aligned with the mesh, the first order upwind discretization may produce erroneous results. The resulting error has a diffusion-like appearance and is referred to as false diffusion (*cf.* §5 of (Versteeg and Malalasekera, 2007)).

The first order generally has better convergence than the second order scheme, but it generally produces less accurate results. Therefore, in this work, it is used the *second order upwind* interpolation scheme.

In second order upwind, the second order accuracy is achieved at cell faces through a Taylor series expansion of the cell-centred solution about the cell centroid (Barth and Jespersen, 1989). The face value ϕ_f is computed using the following expression:

$$\phi_f = \phi + \nabla\phi \cdot \vec{r} \tag{2.40}$$

where ϕ and $\nabla\phi$ are the cell-centered value and its gradient in the upstream cell. This formulation requires the determination of the gradient $\nabla\phi$ in each cell. The gradient is limited so that no new maxima or minima are introduced (ANSYS Documentation, 2013).

Because of its simplicity, this scheme has been widely applied in early CFD calculations. There are other interpolation schemes that can also be considered and used, but they

are not described in this work. For the description of Power Law and QUICK schemes, please refer to §4 in Ferziger and Perić (2002) and §5 in Patankar (1980).

2.2.2 Evaluation of gradients and derivatives

Following ANSYS Documentation (2013), the gradient $\nabla\phi$ of a given variable ϕ is used to discretize the convection and diffusion terms in the flow conservation equations. The gradients are defined according to the Green-Gauss theorem, that states that:

$$(\nabla\phi)_P = \frac{1}{v}\sum_f \overline{\phi}_f \vec{A}_f. \tag{2.41}$$

The value of $\overline{\phi}_f$ is taken from the arithmetic average of the values at the neighbouring cell centers:

$$\overline{\phi}_f = \frac{\phi_P + \phi_N}{2}, \tag{2.42}$$

where ϕ_P refers to the value of ϕ in the center node of the element, P, and ϕ_N refers to the value of ϕ in the center node of one neighbour element, N.

This is called a Green-Gauss cell-based analysis. There are other ways to define the value of $\overline{\phi}_f$, like the Green-Gauss node-based or the Least Squares cell-based analysis, that are not described in this work. For further information about this theme, please refer to ANSYS Documentation (2013).

2.2.3 Discretization of the fundamental equations

After the mathematical method is defined, it is needed to apply a discretization method to the governing equations. The discretization methods consists in approximating the set of partial differential equations by a system of algebraic equations, at some set of locations in space and time (Ferziger and Perić, 2002).

The quality of the numerical solutions is dependent on the quality of the discretizations used. Discretization errors can be reduced by applying the approximations to smaller regions. However, this often implies an increase of computational time and cost of the solution (Ferziger and Perić, 2002).

For transient simulations, the governing equations must be discretized in both space and time. Considering that the problem treated in this work is in a steady state, temporal discretization will be omitted. In the next sections, it is described the discretization of the fundamental equations.

2.2.3.1 Continuity equation

The discrete continuity equation presented in ANSYS Documentation (2013) is given by:

$$\sum_{f}^{N_{faces}} J_f A_f = 0, \tag{2.43}$$

where N_{faces} is the total number of faces, J_f is the mass flux through face f and A_f is the area of the face f. The value of J_f can be determined by the following equation:

$$J_f = \rho_f \frac{a_{p,c0}u_{n,c0} + a_{p,c1}u_{n,c1}}{a_{p,c0} + a_{p,c1}} + d_f\left((p_{c0} + (\nabla p)_{c0} \cdot \vec{r}_0) - (p_{c1} + (\nabla p)_{c1} \cdot \vec{r}_1)\right), \tag{2.44}$$

where p_{c0} , p_{c1} and $u_{n,c0}$, $u_{n,c1}$ are the pressures and normal velocities respectively, within the two cells on either side of the face, and the term d_f is a function of $\overline{a}_P$, the average of the momentum equation a_P coefficients for the cells on either side of the face f (ANSYS Documentation, 2013).

2.2.3.2 Navier-Stokes equations

Given a pressure field p, the discretized momentum equations can be written for each control volume and then solved to obtain the velocity fields. The discrete Navier-Stokes equations is obtain by setting $\phi = u, v, w$ in Eq. (2.35). ANSYS Documentation (2013) presents the momentum equations as:

$$a_P u = \sum_{nb} a_{nb}u_{nb} + \sum p_f A \cdot \hat{i} + S_x, \tag{2.45}$$

$$a_P v = \sum_{nb} a_{nb}v_{nb} + \sum p_f A \cdot \hat{j} + S_y, \tag{2.46}$$

$$a_P w = \sum_{nb} a_{nb} w_{nb} + \sum p_f A \cdot \hat{k} + S_z, \tag{2.47}$$

where a_{nb} represents the influence coefficient of the neighbouring cells and can be calculated using the upwind scheme, suitable for convection–diffusion problems. These coefficients contain combinations of the convective flux per unit mass and the diffusive conductance at the control volume cell faces (Versteeg and Malalasekera, 2007). The value of a_P represents the center coefficient of the cell.

If the pressure field and face mass fluxes are not known *a priori*, they must be obtained as a part of the solution. The pressure field is extracted by solving a pressure or pressure correction equation which is obtained by manipulating continuity and momentum equations (Ferziger and Perić, 2002).

There are several pressure interpolation schemes, such as Standard (Rhie and Chow, 1983), Second Order or Body Force Weighted. (Patankar, 1980). In this work, the second order scheme was considered. As it is explained before, the pressure is modelled using a central differencing scheme. ANSYS Documentation (2013) describes it as can be seen in Eq. (2.48). The pressure face values are given by:

$$P_f = \frac{1}{2}(P_{C0} + P_{C1}) + \frac{1}{2}(\nabla P_{C0} \cdot \vec{r}_{C0} + \nabla P_{C1} \cdot \vec{r}_{C1}). \tag{2.48}$$

2.2.4 SIMPLE algorithm

In incompressible flows, density is constant and therefore not linked to pressure. In this case, coupling between pressure and velocity introduces a constraint in the solution of the flow field: if the correct pressure field is applied in the momentum equations the resulting velocity field should satisfy continuity (Ferziger and Perić, 2002).

The problems associated with the non-linearities in the equation set and the pressure–velocity linkage can be resolved by adopting an iterative solution strategy. In this work, the iterative method used is SIMPLE algorithm, and therefore it is here briefly described. However, there are other pressure-velocity coupling algorithms, like SIMPLER (Patankar, 1980), SIMPLEC (Vandoormaal and Raithby, 1984) or PISO (Issa, 1986) that can be also applied.

SIMPLE is an acronym for **S**emi-**I**mplicit **M**ethod for **P**ressure **L**inked **E**quations. It was first proposed by Patankar and Spalding (1972). The full description of this algorithm can be consulted in §6.7 of Patankar (1980).

In this algorithm, the convective fluxes per unit mass F through cell faces are evaluated from so-called guessed velocity components. A guessed pressure field is used to solve the momentum equations, and a pressure correction equation, deduced from the continuity equation, is solved to obtain a pressure correction field, which is in turn used to update the velocity and pressure fields (Versteeg and Malalasekera, 2007).

Chapter 3

Numerical model of the *Transformers' room*

Abstract

In this chapter, the construction of the numerical model of the Transformers' room is presented. The description of this case can be consulted in § 1.2.1. The purpose of this model is to simulate the air flow and air temperature inside the room, regarding the effects of all the heat sources. The results are presented at the end of the chapter.

3.1 Geometry

The first step to create a numerical model is to build a geometry that represents the case in study. The building process of the geometry is of the most importance. The closest the geometry is to the real case, the more accurate the results tend to be.

For creating a model the closest possible to the real case, it is important to know the real dimensions of the room and its equipments. For this effect, the project blueprints were consulted. In complement, real scale measures were taken on the field, in order to confirm and clarify some of dimensions missing on the blueprints.

All device elements that were important to the investigated physical processes were maintained in their original shapes and dimensions.

The main difficulty with the geometry creation for this model resulted from the several different scales. The model had to consider elements as the transformers' fins that were

very thin (few millimetres), compared with the dimensions of the other equipments and the room itself.

Due to its importance, a lot of time was invested in the full definition of the geometry during this work. As a result of this process, the geometry of the interior of the room was drawn using SolidWorks®, and it is presented on Figure 3.1.

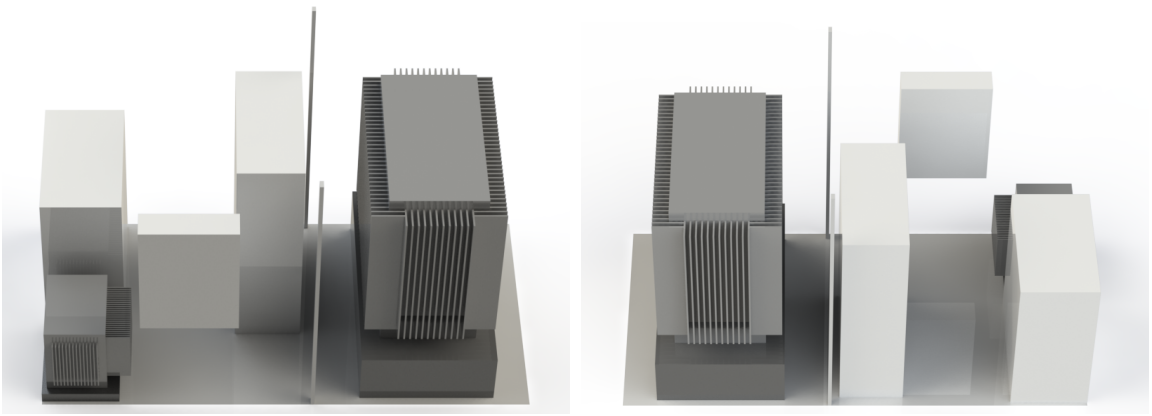

(a) View from the front wall. (b) View from the back wall.

Figure 3.1: Representation of the interior equipments of *Transformers' room*.

In Figure 3.2 it is possible to identify all the elements modelled inside the *Transformers' room*:

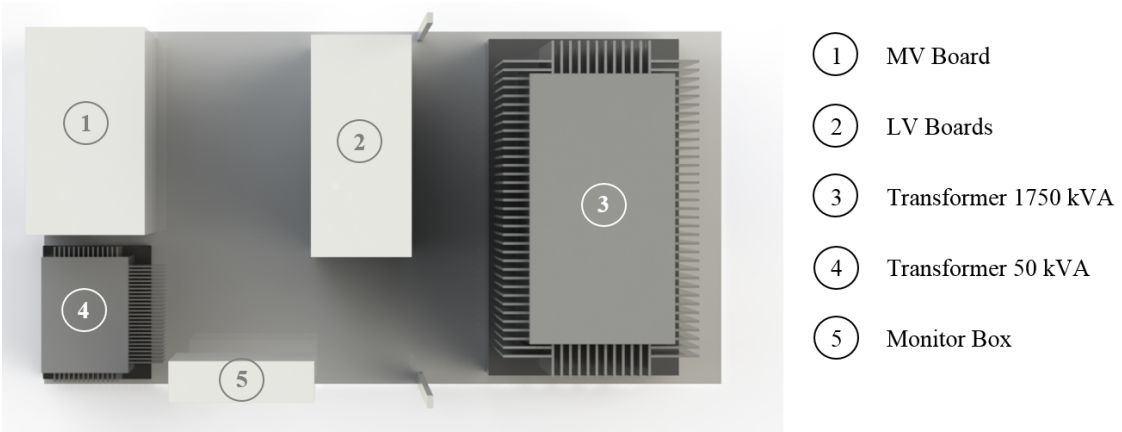

Figure 3.2: Identification of the equipments inside the *Transformers' room*.

It must be stated that the main objective of this work is to analyse the air flow and local temperature inside the room, not the intrinsic behaviour of each equipment. Therefore, the geometry of the numerical model must be a representation of the domain where the air is flowing inside the *Transformers' room*.

In order to obtain this representation, it was created another geometry, featuring the length, width and height of the *Transformers' room*. Using the command *Combine* on SolidWorks®, it was possible to subtract the bodies of the elements inside from this last geometry, creating a kind of air's male mold of the room.

This geometry became fully defined with the representation of the air entrance grids on the front, back and side walls, the box of the ventilator on the back wall and the air entrance and ventilator grids of the *LV Boards*. Therefore, the final geometry is presented on Figure 3.3.

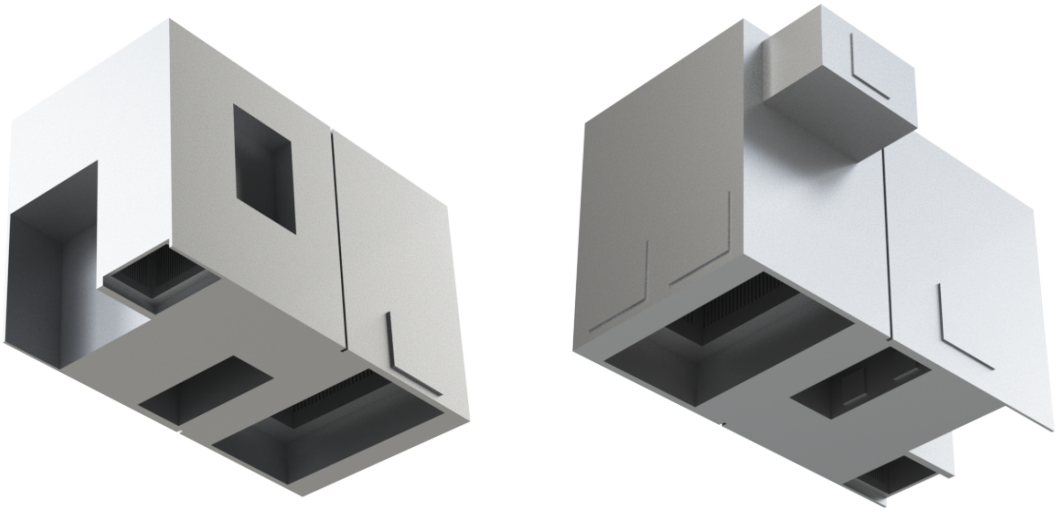

(a) View from the front wall (b) View from the back wall

Figure 3.3: Representation of the air inside the *Transformers' room*.

The SolidWorks® file was then loaded into the *Fluent Fluid Flow* analysis file in ANSYS® *Workbench* environment. Using the ANSYS® *Design Modeller* program, the geometry file was regenerated and converted into one single body, and this body was defined as a fluid.

3.2 Computational mesh

After the full definition of the geometry, a computational mesh needs to be created. According to Ferziger and Perić (2002), the computational mesh is a division of the solution domain into a finite number of subdomains (the control volumes), on which the fundamental equations will be solved.

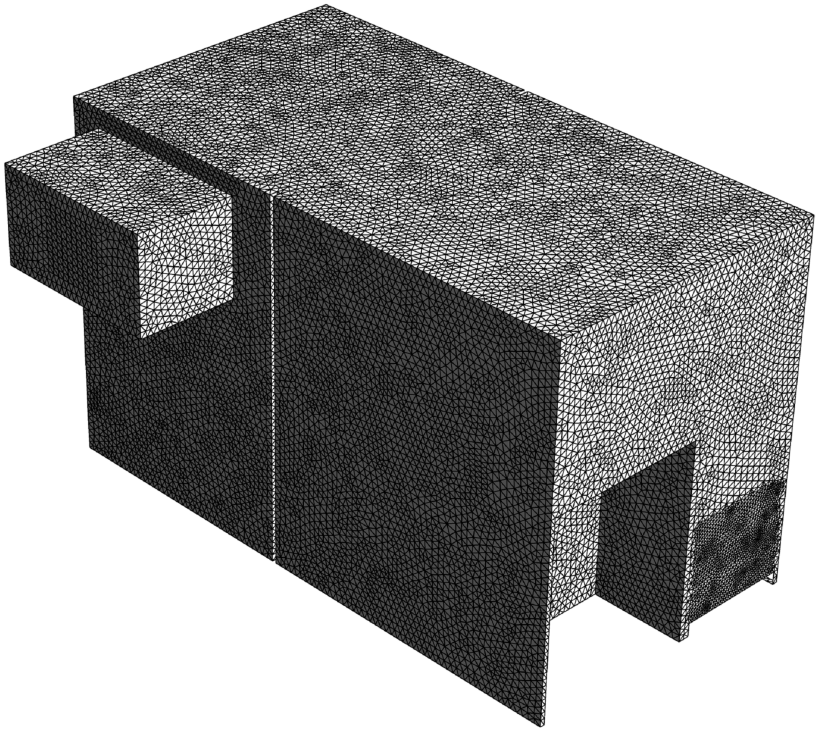

(a) Back wall view.

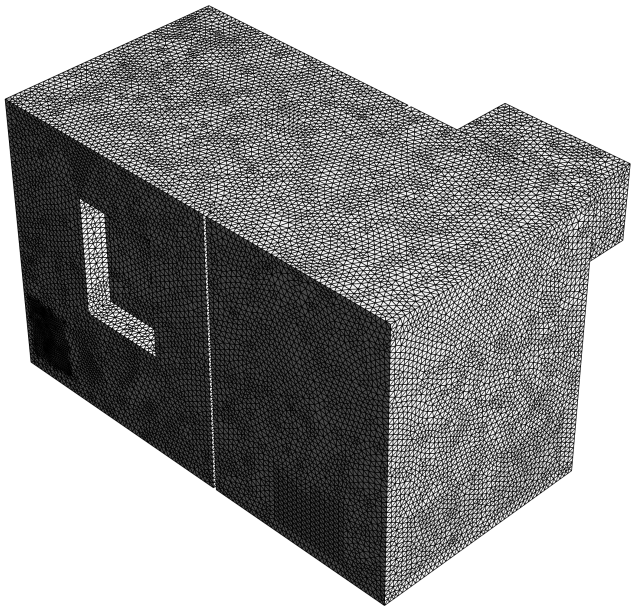

(b) Front wall view.

Figure 3.4: Computational mesh generated based on the geometry model.

The mesh generation is a process that consumes a lot of time. However, it must be considered that the quality of the solution depends as much on the mesh quality as on the numerical model (Versteeg and Malalasekera, 2007).

Before starting the mesh generation process, there are some aspects that must be considered. One of them is the shape or type of the elements. The most popular types are triangular (2D) or tetrahedra (3D) elements, because they are easier to automatic generate. However, it must be regarded that it can be the cause of unexpected problems. For example, tetrahedra elements are not desired in a near wall analysis if the boundary layer must be resolved (Ferziger and Perić, 2002).

Another aspect to take in account is the elements size. The accuracy of the approximation to the surface and volume integrals is better when this size is refined, which leads to a reduction of discretization errors. Also, large ratio sizes of the adjacent cells can affect accuracy, so it is important to restrain it (Ferziger and Perić, 2002).

In this work, three different meshes were created, with correspondence to coarse, medium and fine element sizes. Their characteristics are presented on Table 3.1. It was not feasible to refine the element size on the finest mesh due to hardware limitations. The generation of the finest mesh in the transformers' geometry was difficult and required a high number of elements. The numerical model with such a large mesh size was solved using parallel processing.

Table 3.1: Properties of the computational meshes of the *Transformers' room*.

	Coarse	*Medium*	*Fine*
Element type	Tetrahedrons	Tetrahedrons	Tetrahedrons
Element size [m]	0.072	0.060	0.050
Elements	1119032	1621689	2619094
Nodes	229506	324788	519423
Growth rate	1.2	1.2	1.2

All the meshes were generated having as basis the geometry presented in § 3.1, using the program ANSYS® *Meshing* from the ANSYS® *Workbench* environment. The one used in this work corresponds to the finest case, and it is presented on Figure 3.4.

The last step using ANSYS® *Meshing* program is to group and name the faces of the mesh which will have the same boundary conditions. Although this is made with the ANSYS® *Meshing* program, the complete definition of the boundary conditions will only be done using ANSYS® *Fluent*.

3.3 Boundary conditions

In this section it is presented the air flow and thermal boundary conditions considered at the limits of the computational domain. These limits are presented on Figure 3.5, Figure 3.6, Figure 3.7 and Figure 3.8.

At the walls, the no-slip condition is applied, *i.e.* the velocity of the fluid is equal to the wall velocity. In this work, all walls are considered stationary.

To define the turbulence boundary conditions, the hydraulic diameter of each inlet and outlet was calculated and it was defined a turbulence intensity value of 5%. Turbulence intensity is the ratio between the root-mean-square of the turbulent velocity fluctuations u' and the mean velocity U. The value of 5% represents a medium intensity scenario, and it is the default value in ANSYS Documentation (2013).

The entrance grids on the front, back and side wall were modelled as pressure inlets, and therefore no velocity condition was defined in these sections. The temperature of the air entering through these surfaces is equal to the exterior temperature considered (30 °C).

The outlet ventilator surface was modelled with the definition of the normal velocity. This was used to accomplish the ventilator's volume flow rate operating conditions. Based on the surface area value, it was defined a normal velocity of -6.11 m/s (from the interior to the exterior of the domain).

Both the transformers were considered as walls. Like the container's external walls, floor and roof, an uniform heat flux was imposed, based on the values of Table 1.1 and the area of the walls.

The *MV Board* and the *Monitor Box* were considered as adiabatic walls. The *LV Boards* walls were also defined as adiabatic. Normal velocity conditions were imposed on both inlets (-4.56 m/s) and outlets of the board (2.28 m/s). The values were also calculated from the volume flow rate and inlet and outlet surface area. The air temperature on the outlets was also defined (33.62 °C), in order to guarantee the 1700 W heat generation of the equipment.

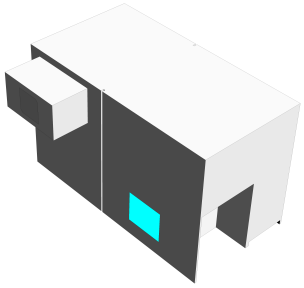

(a) Air inlet back door.

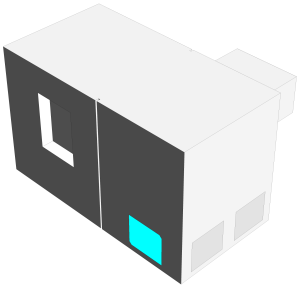

(b) Air inlet front door.

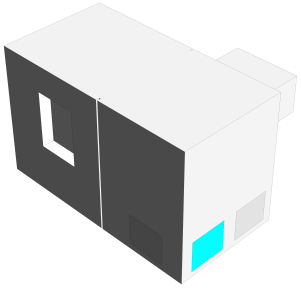

(c) Air inlet side wall 1.

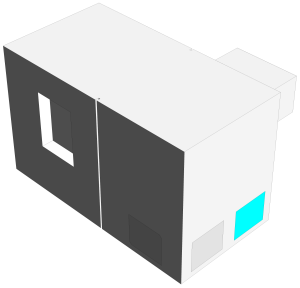

(d) Air inlet side wall 2.

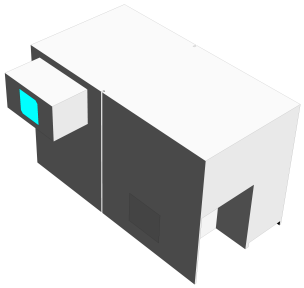

(e) Air outlet ventilator.

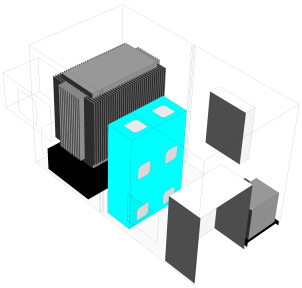

(f) *LV Boards*.

Figure 3.5: Representation of the boundaries of the numerical model. (1)

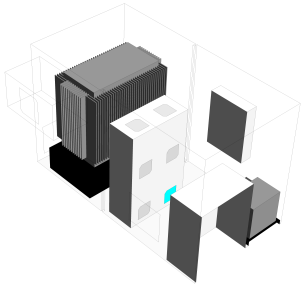

(a) *LV Boards* inlet 1.

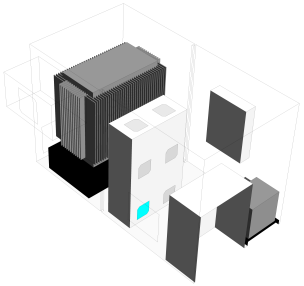

(b) *LV Boards* inlet 2.

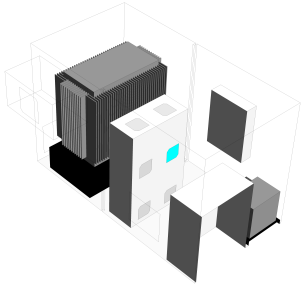

(c) *LV Boards* door outlet 1.

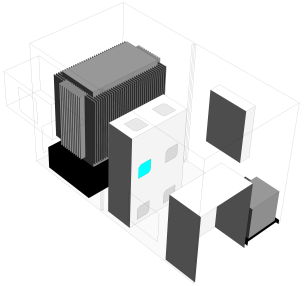

(d) *LV Boards* door outlet 2.

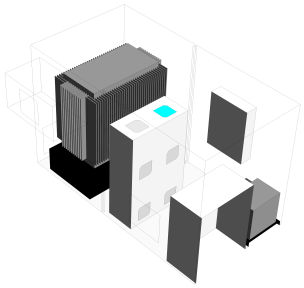

(e) *LV Boards* top outlet 1.

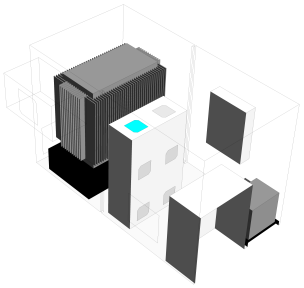

(f) *LV Boards* top outlet 2.

Figure 3.6: Representation of the boundaries of the numerical model. (2)

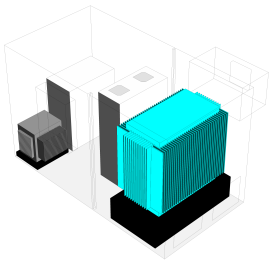

(a) *Transformer 1750 kVA*.

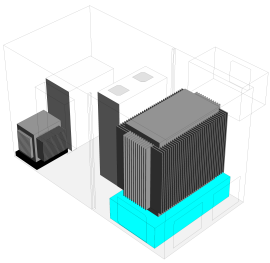

(b) *Transformer 1750 kVA* tank.

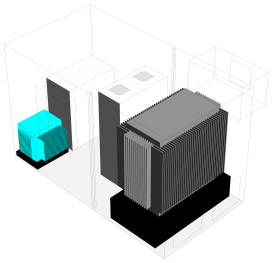

(c) *Transformer 50 kVA*.

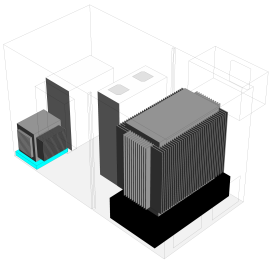

(d) *Transformer 50 kVA* base

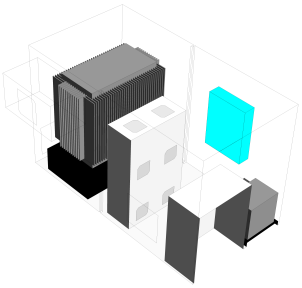

(e) *Monitor box*.

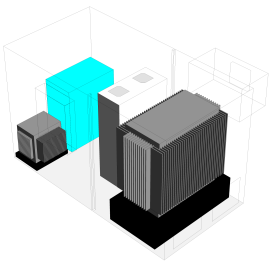

(f) *MV Board*.

Figure 3.7: Representation of the boundaries of the numerical model. (3)

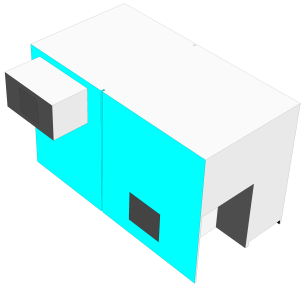

(a) Back wall.

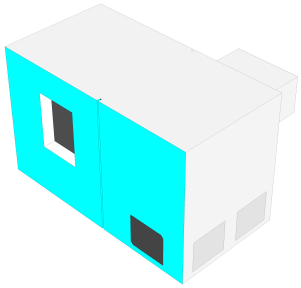

(b) Front wall.

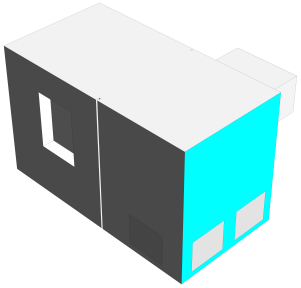

(c) Exterior side wall.

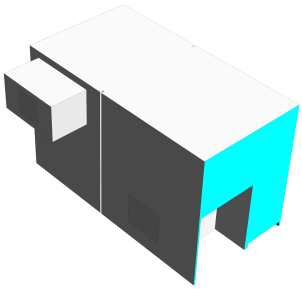

(d) *Inverters' room* side wall.

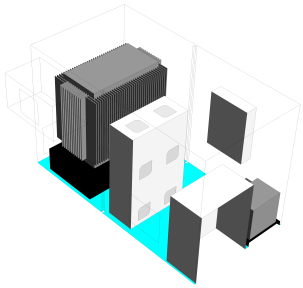

(e) Floor.

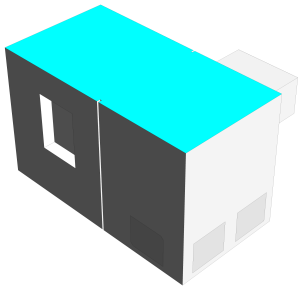

(f) Roof.

Figure 3.8: Representation of the boundaries of the numerical model. (4)

3.4 Properties of the materials

While building the numerical model in ANSYS® *Fluent* and defining the boundary conditions, one must also specify the fluid and the materials in what the boundary walls are made of. In this work, the fluid is air. In addiction to this, another two different materials were considered. The two transformers are essentially made of steel, while the *MV Board*, *LV Boards*, *Monitor Box*, as well as the container's walls, roof and floor, are made of aluminium.

In the following table it is possible to consult the values of density, specific heat, thermal conductivity and viscosity of air, steel and aluminium. These were the default values set by the program.

Table 3.2: Physical and thermal properties of the materials (ANSYS® *Fluent*).

	ρ $[kg/m^3]$	c_p $[J/kg \cdot K]$	k $[W/m \cdot K]$	μ $[kg/m \cdot s]$
Air	1.23	1006.43	2.42×10^{-2}	1.79×10^{-5}
Steel	8030	502.48	16.27	-
Aluminium	2719	871	202.4	-

3.5 Verification and validation of the model

Validation is the process of determining the degree to which a model is an accurate representation of the real situation in study. The validation of the computational results obtained from the developed mathematical model must imply experimental data or already validated computational results (Versteeg and Malalasekera, 2007).

First of all, it must be stated that the evaluation of the accuracy is enhanced by a detailed definition of the problem geometry and boundary conditions. A sufficiently credible validation must be based in trustful experimental information (Versteeg and Malalasekera, 2007).

This information relates to detailed measurements of distributions of flow properties, such as velocity and temperature. As complement, it can also be measured the mass flow rate or the total heat transferred. However, it must be also stated that the experimental data likely has uncertainties and errors associated with it.

The model is said to be validated when the difference between the numerical results and the experimental data is lower than a certain value. However, this criterion is somehow subjective, and some more rigorous validation methods were proposed by Coleman and Stern (1997) and Oberkampf and Trucano (2002).

A complete validation analysis is supposed to include an examination to iterative, spacial (and temporal, if it is the case) convergence, an examination to the consistency of the simulation results, a comparison between CFD results and experimental data and the analysis of the model uncertainties.

In order to validate the computational simulation results of this work, a complete on-field measuring program was conceived. This protocol included velocity and temperature measurements in all inlets and outlets of the container, as well as the inlets and outlets of the *LV Boards*. It included also measurements of temperature on the surfaces of both the transformers, along with thermographic profiles of the interior of the room.

However, it was impossible to perform these measurements and compare with the CFD results. Therefore, it must be said that the model presented in this work is not validated.

The verification of the results is performed with the analysis of the convergence of the numerical solution, and the evaluation of the grid independence of the results, which are presented in the next sections.

3.5.1 Convergence of the numerical solution

A numerical method is said to be converged if the solution of the discretized equations tend to the exact solution of the differential equation as the grid spacing tends to zero (Ferziger and Perić, 2002).

Despite its importance, there are actually no universal and foolproof methods to conclude if the solution of the model has converged or not.

One effective and useful indicator is the evaluation of the scaled residuals. The calculation of the residuals can be consulted in ANSYS Documentation (2013).

Usually, the analysis of the behaviour of the residuals is sufficient to conclude about the convergence of the solution. For higher levels of precision, the convergence can be evaluated by monitoring integral quantities (for example, overall heat transfer coefficient) (ANSYS Documentation, 2013).

At the end of each solver iteration, the residual sum for each of the conserved variables is computed and stored, and therefore the convergence history is recorded. Its evolution is plotted and can be monitored in real time.

The iterative calculations are meant to stop after a programmed number of iterations, defined by the user, or after the values of the scaled residuals satisfies a convergence criterion.

In this work, the convergence criteria considered requires that the globally scaled residuals for each equation decrease to the values presented on Table 3.3. Once the scaled residuals get lower than these values, the solution is said to have converged.

The evolution of the scaled residuals can be seen on Figure 3.9.

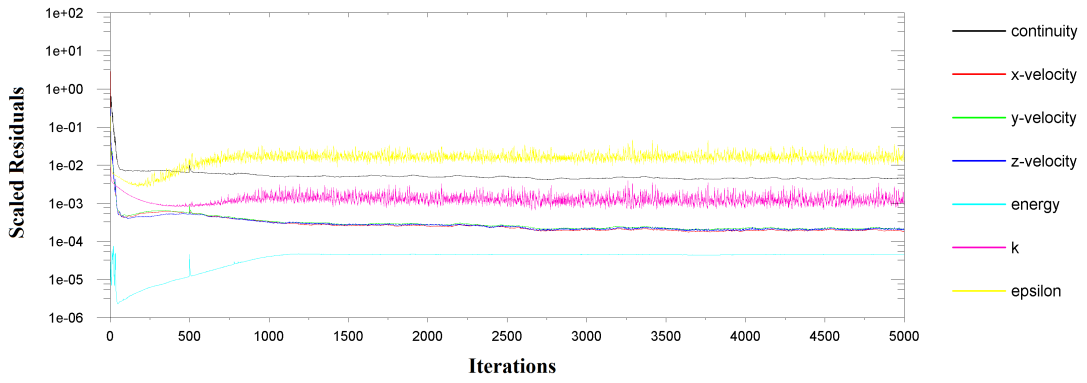

Figure 3.9: Evolution of the scaled residuals.

In Table 3.3 it is possible to observe the values of the scaled residuals at the end of 5000 iterations.

The convergence should be evaluated not just from the value of the residual itself, but from its behaviour. The natural behaviour of the residuals implies the decay to some small value (“round-off”) and then stop changing (“level out”).

From the analysis of the Figure3.9 and Table 3.3 it is possible to conclude that the residuals of x,y, and z-velocities tend to a stable value at the end of the first 100 iterations, and satisfy the convergence criteria.

The residual of the continuity equation present the same behaviour, but it does not tend to a value lower than its convergence criterion. This fact can be related with the need of a more accurate definition of the velocities on both inlet and outlet boundaries of the model.

Table 3.3: Convergence criteria and scaled residuals values.

	Convergence criteria	Scaled residuals
Continuity	10^{-3}	4.5475×10^{-3}
x-velocity	10^{-3}	1.7974×10^{-4}
y-velocity	10^{-3}	2.0772×10^{-4}
z-velocity	10^{-3}	1.4384×10^{-4}
Energy	10^{-6}	4.4514×10^{-5}
k	10^{-3}	9.2610×10^{-4}
ε	10^{-3}	1.3994×10^{-2}

The residuals of the k and ε equations present an highly oscillatory behaviour, which may indicate that the turbulence model considered may no be the most indicated. Although the residual of the k equation have met the convergence criterion, the one of the ε equation is still far from that value. Further works in this field should evaluate the sensibility of the results to different turbulence models.

The residual of the energy equation is dropping in the beginning of the calculations, but then increases and stalls. As it is possible to observe, although it has the lowest residual value of the seven equations, it has not met its convergence criterion.

It must be stated that these behaviours can be also related to bad mesh quality, and would be mitigated if a higher quality mesh was used. However, due to hardware limitations, this was not feasible in this work.

3.5.2 Evaluation of the grid independence

In this section, the grid independence of the mathematical model is evaluated. One significant issue in numerical computations is what level of grid resolution is appropriate. This is a function of the flow conditions, type of analysis, geometry, and other variables.

It is common to begin the numerical simulations with a grid resolution and then conduct a series of grid refinements to evaluate the effect of grid resolution. As the grid is

refined (grid cells become smaller and the number of cells in the flow domain increases), the spatial discretization errors should asymptotically tend to zero.

Methods for examining the spatial and temporal convergence of CFD simulations are presented in Roache (1994), and they are based on the Richardson's extrapolation. Roache (1994) suggests the determination of a grid convergence index (GCI) to provide a consistent manner in reporting the results of grid convergence studies and perhaps provide an error band on the grid convergence of the solution.

The GCI is a measure of the percentage the computed value is away from the value of the asymptotic numerical value. It indicates how much the solution would change with a further refinement of the grid. A small value of GCI indicates that the computation is within the asymptotic range.

Therefore, the GCI is used to determinate the discretization error by comparing the results for the three different meshes. The results of the evaluation are present on Table 3.4.

Table 3.4: Grid independence analysis of the results.

		Mass flow rate $[kg/s]$	Total heat transferred $[W]$	Average temperature $[^{\circ}C]$
Variable values	ϕ_1	1.66	26456.03	39.48
	ϕ_2	1.68	25561.94	39.58
	ϕ_3	1.68	25992.37	38.89
Absolute differences	α_{21}	0.0164	-894.0910	0.0947
	α_{32}	0.0026	430.4260	-0.6882
Order of convergence	p	-2.6771	-1.0547	2.8619
Factor of safety	F_S	1.25	1.25	1.25
GCI [%]	GCI_{21}	-1.4603	-8.1460	0.0478
	GCI_{32}	-0.2261	-4.0588	0.3467

The mass flow rate, total heat transferred and volume averaged air temperature were considered in this evaluation. From the analysis of Table 3.4, it is possible to conclude that the results of GCI are acceptable when compared to other values on literature in a similar kind of study (Ramos et al., 2013).

The mesh used in this work is the finest (third case), and as it is possible to observe, the GCI results indicate that there is a maximum error of 4.06% (regarding the total heat transferred value) emerging from the spacial discretization and grid refinement, from the second mesh to the third. Comparing with the results of Ramos et al. (2013), this value is considered low enough and acceptable, and therefore it is possible to conclude that this error will have little impact on the final solution of the model.

3.6 Analysis of the results

After the conception of the geometry, the generation of the computational mesh, the input of the operating and boundary conditions and the definition of solution methods, it is possible to numerically solve the model.

In this work, the solution of the model was obtained with ANSYS® *Fluent*, using an Intel® Core i7-3537U CPU at 2.0 GHz, with 4 GB of RAM memory.

3.6.1 Air flow inside the room

The air flow profile obtained from the numerical simulation can be seen on Figure 3.10 and Figure 3.11.

The mass of air is set in motion by the action of the ventilator, installed on the back wall. Although it was modelled to guarantee the volume flow rate condition (by the imposition of the normal velocity), the physical phenomenon that triggers the air flow is based on the pressure difference introduced by the ventilator.

Due to this gradient of pressure, the air is forced his way into the container through the grids on its walls. As it was explained before, there are four grids. Their volume flow rates were computed and the values are resumed on Table 3.5.

Combining the analysis of Figure 3.10 and Figure 3.11 and Table 3.5 data, it is possible to conclude that the *Transformer 1750 kVA* is potentially blocking the entrance of air from the inlets on the side wall and front door. The volume flows passing through these

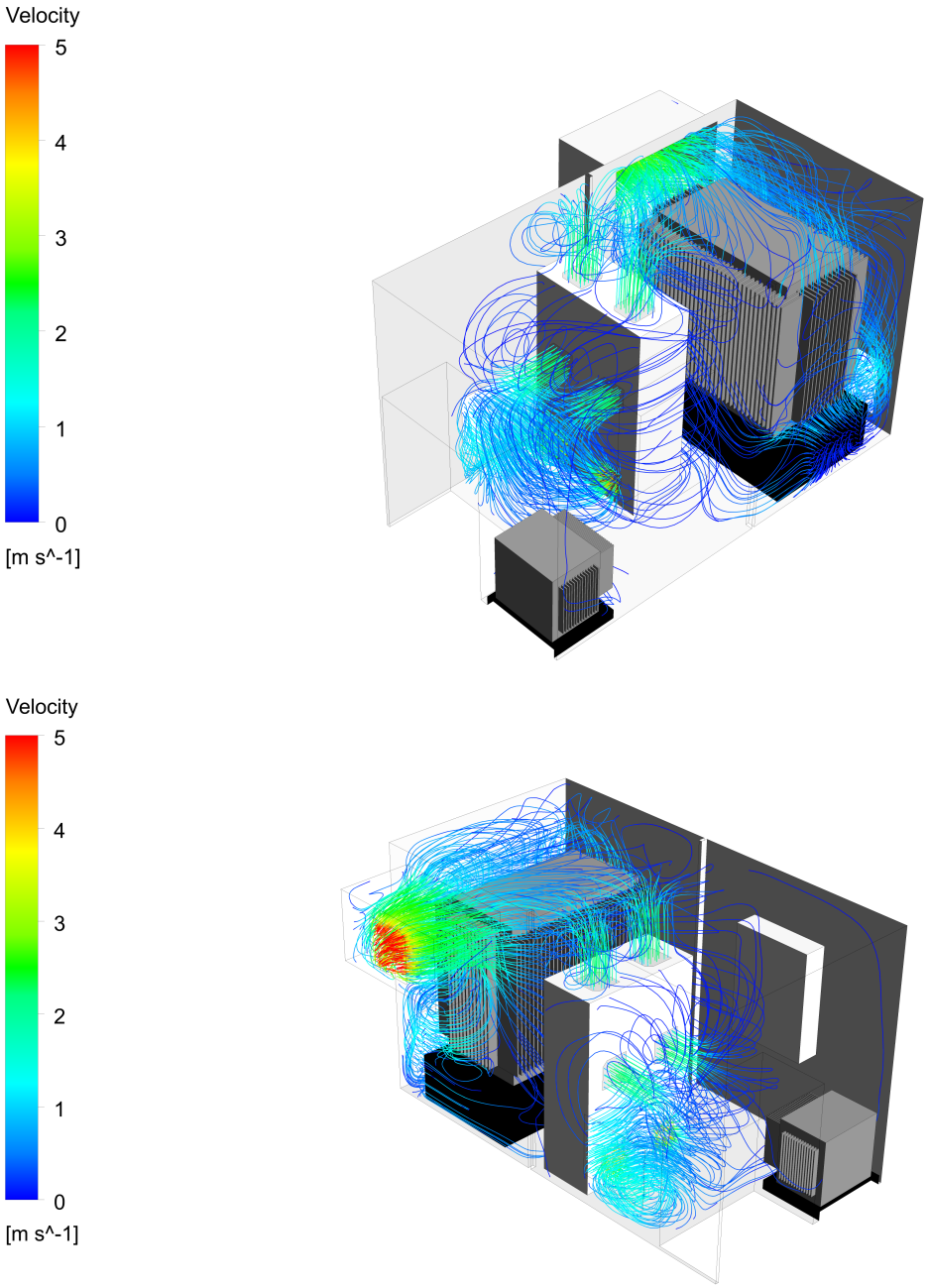

Figure 3.10: Representation of the air flow inside the *Transformers' room*. (1)

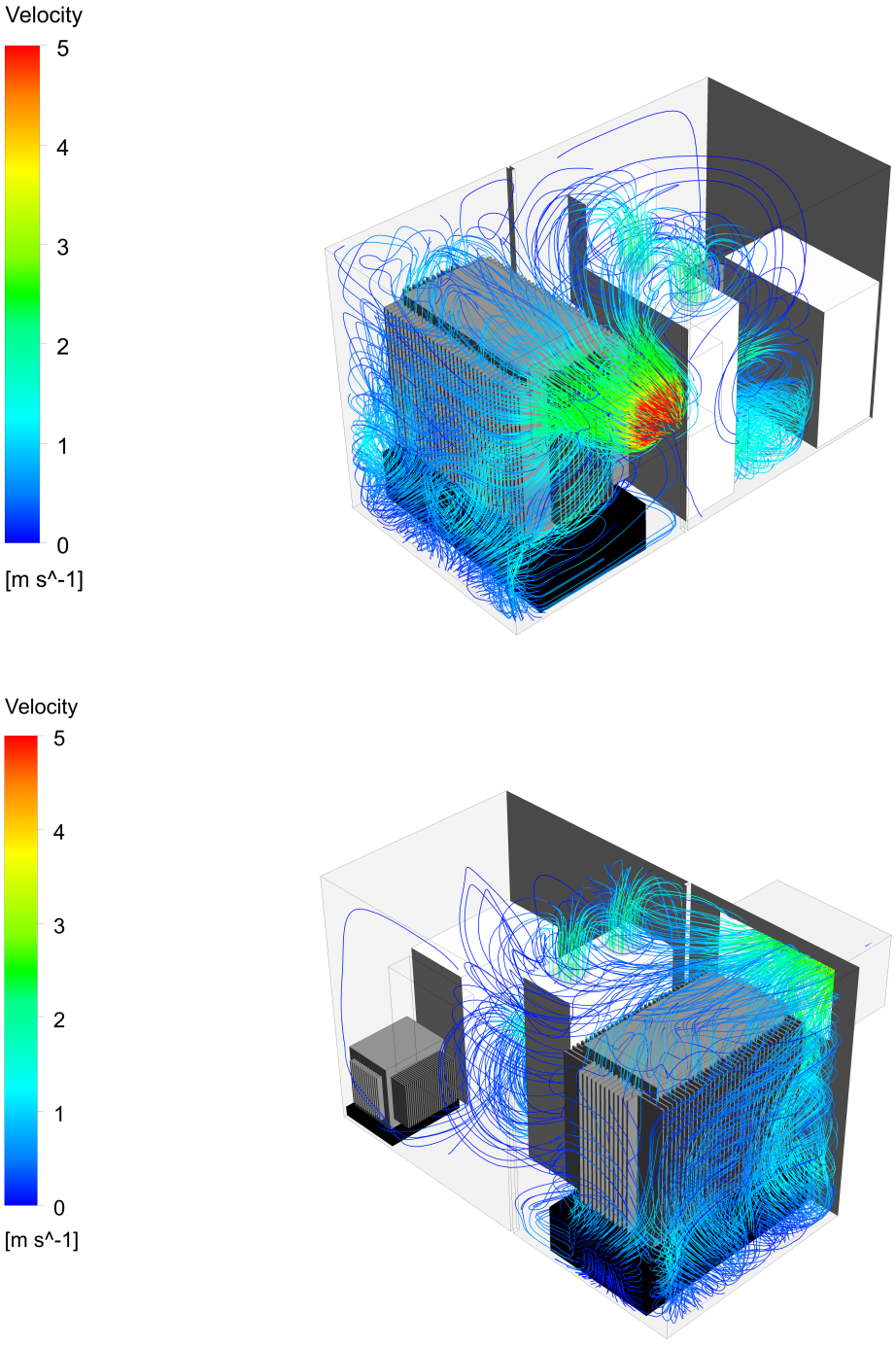

Figure 3.11: Representation of the air flow inside the *Transformers' room*. (2)

Table 3.5: Values of volume flow rate on the inlets and outlets of the *Transformers' room*.

	Volume flow rate [m^3/s]
Air inlet front door	0.178
Air inlet back door	0.652
Air inlet side wall 1	0.271
Air inlet side wall 2	0.341
Air outlet ventilator	-1.513

faces are substantially lower that the one of the back door inlet, which is not blocked by any equipment.

The short distance between the transformer and the inlets affect not only the pattern of the fluid flow but also the velocities of the air in those regions. The velocity of the air will have influence on the heat transfer process, as convection depends significantly on it.

The air entering through the front door and side wall inlets has the tendency to flow around the wall side of the transformer and go directly to the ventilator.

The major quantity of the air entering through the back door inlet is flowing towards the *LV Boards* inlets. However, as it is possible to observe, the remaining air tends to go around the *LV Boards* on way to the ventilator. This leads to the existence of regions where the air is not in motion. These regions comprehend essentially the vicinity of the *Transformer 50 kVA* and *MV Board*.

The *LV Boards* internal ventilation system has a substantial influence on the air flow inside the room. This will be properly evaluated in § 3.6.5.

3.6.2 Thermal distribution inside the room

The numerical simulation of the thermal distribution of the air inside the *Transformers' room* are presented in Figure 3.12 and Figure 3.13.

From the analysis of Figure 3.12 and Figure 3.13 it is possible to conclude that there are four distinct temperature regions inside the room. Three of these regions are in the

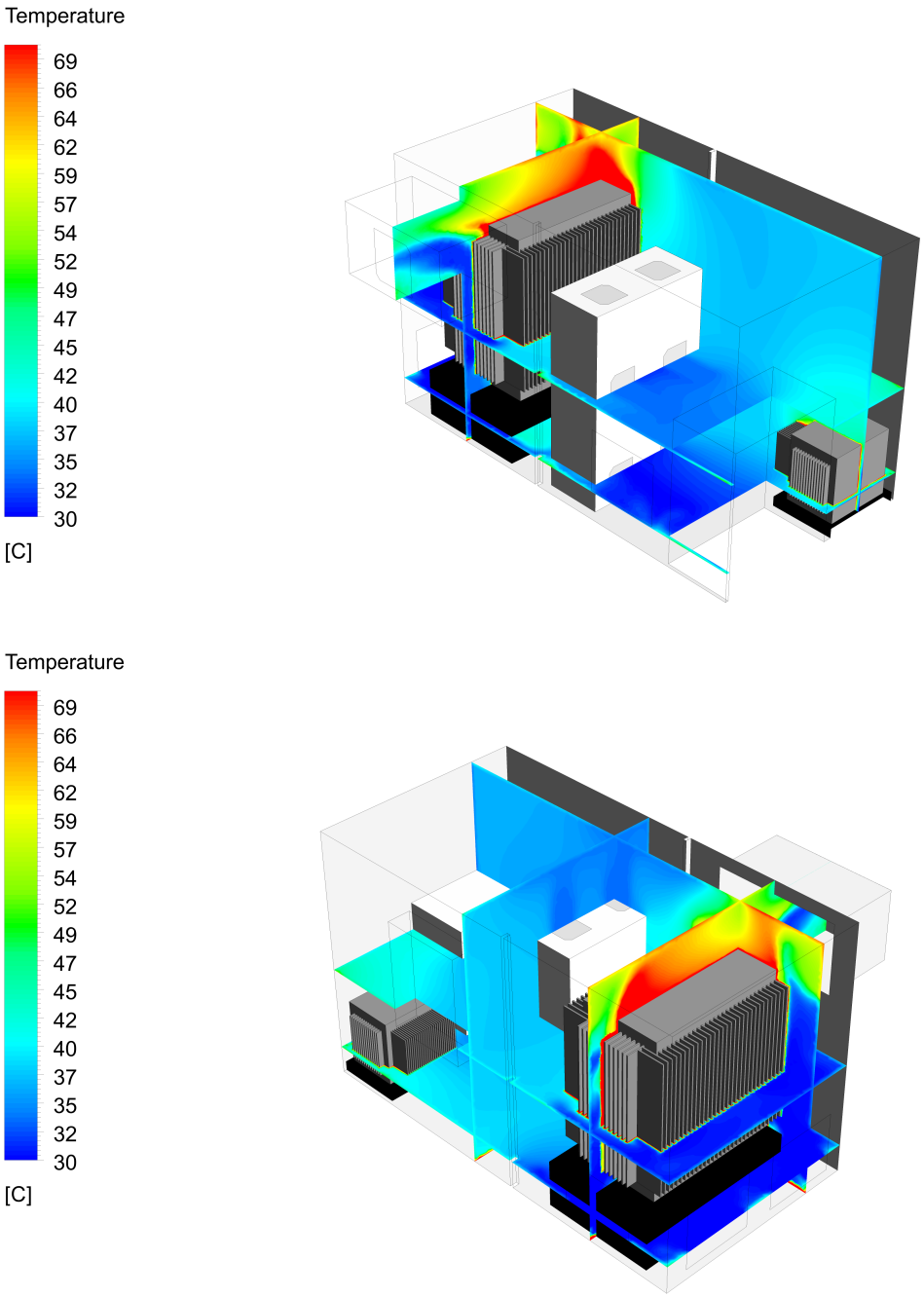

Figure 3.12: Representation of the air temperature distribution inside the *Transformers' room*. (1)

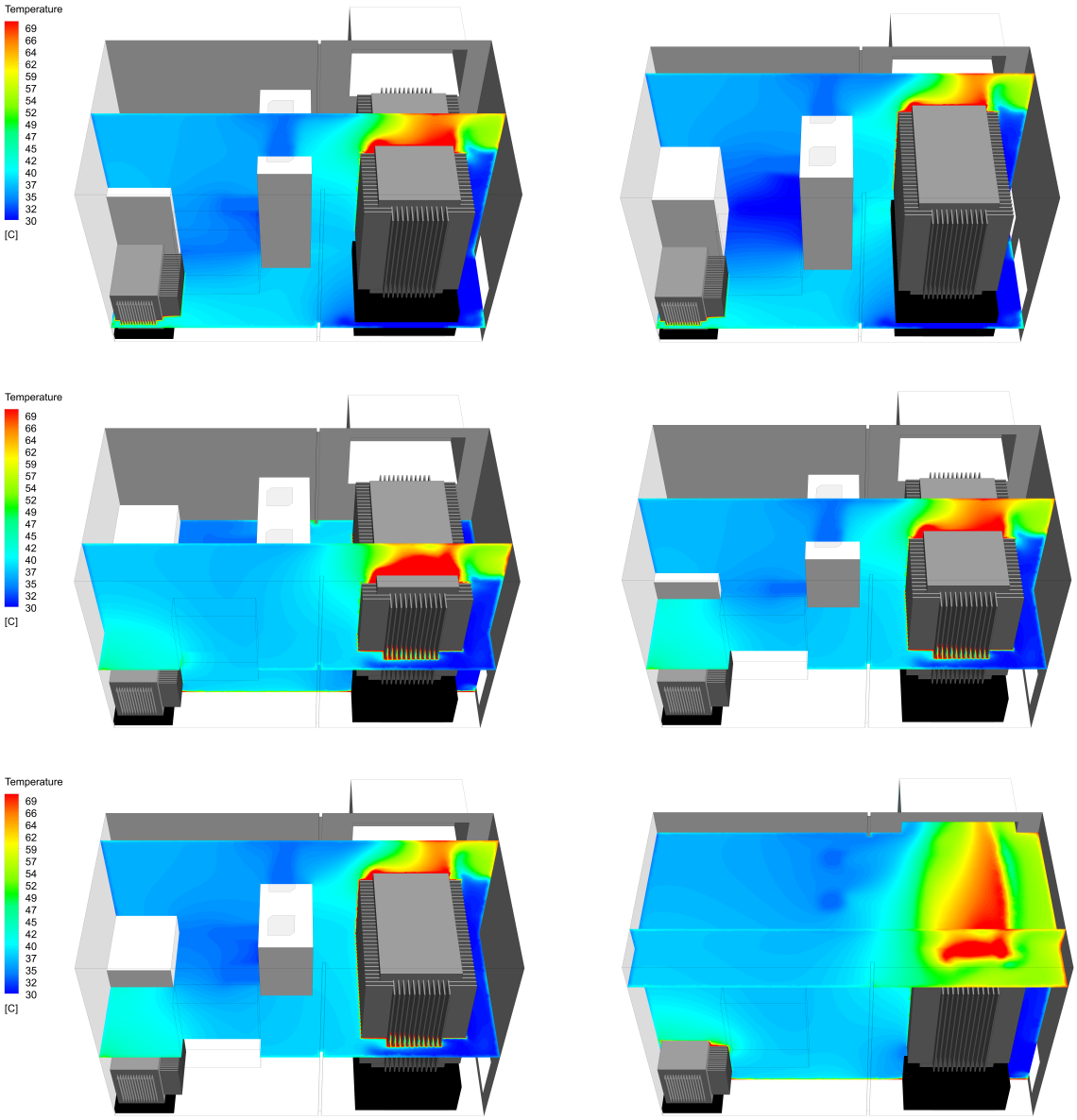

Figure 3.13: Representation of the air temperature distribution inside the *Transformers' room*. (2)

vicinity of the *Transformer 1750 kVA*, while the other one is on the vicinity of the *Transformer 50 kVA*. The thermal analysis of these two equipments is presented further on this work (*cf.* § 3.6.3 and § 3.6.4).

In a previous note, it must be stated that the *Transformer 1750 kVA* is the largest heat generator of the system, and the temperatures on its surfaces register the highest values of the model (approximately 120 °C). Hence, it is the equipment that influences the most the air temperature distribution.

The highest values of air temperature are registered immediately on the top of it, as it is possible to see from the figures. Unlike the fins, the top surface is the most difficult section to cool. This happens because the majority of the air entering the container is first passing through the fins. The air temperature will therefore increase, and due to the decrease of the difference of temperatures, the heat transferred by convection on the top surface will be lower.

By contrast, the air next to the transformer's fins is almost at the initial entrance temperature. Due to the proximity of the inlets and the tight space between the transformer and the walls, the air velocity is higher in these region, which means that the air renewal rate here is higher than in the rest of the room and, in steady state conditions, the temperature will tend to the entrance value.

The heat generation of the transformer is also influencing the air temperature in the space between the first and the *LV Boards*. As the air that enters through the inlet on the back door tends to be aspired by the inlets of the *LV Boards*, only a small share is forced to go around the board. Therefore, the local air renewal rate is low and the heat transferred on the transformer's fins from that side tends to increase the local air temperature (approximately 42 °C).

On the other end of the room, the heat generation of the *Transformer 50 kVA* combined with the low values of the local velocity, originate a region of hot air with temperatures around 45 °C, on the transformer's corner.

The coolest regions are adjacent to the air inlets on the side wall and on the front and back doors. Here, the temperature of the air is still not affected by the heat sources inside the container, and therefore it is almost the same as the temperature on the outside (approximately 30 °C).

A quick analysis of the thermal profiles allows to conclude that the most of the air is at a temperature around 39 °C. In order to confirm this statement, a volume averaged air temperature inside the room was computed, and the result is presented on Table 3.6:

Table 3.6: Volume averaged temperature inside the *Transformers' room*.

Volume averaged air temperature [$^{\circ}C$]	38.89

3.6.3 Thermal analysis of the *Transformer 1750 kVA*

As it was said before , the *Transformer 1750 kVA* is one of the key elements in the thermal analysis of the room, and therefore shall be studied in more detail.

The Joule effect and the Foucault currents produce heat in the different internal components of the transformer. From the economical and safety points of view, there is a need to cool the transformer in order to preserve it from destruction.

The transformer has an internal cooling system that will not be considered on this simulation. Only the heat transfer on the transformer's fins will be analysed.

The thermal distribution profiles can be seen in Figure 3.14 and Figure 3.15. Table 3.7 present the computed values of average surface temperature, average heat transfer coefficient and total heal transferred on the surfaces of the transformer.

Table 3.7: Computed thermal and heat values of the *Transformer 1750 kVA*.

Average surface temperature [$^{\circ}C$]	63.50
Average heat transfer coefficient [$W/m^2/^{\circ}C$]	4.58
Total heat transferred [kW]	20.90

Note that, as it was explained in § 3.3, the heat produced by every active part of the transformer was defined to be uniformly distributed on its surfaces. This includes the fins and the top surface.

The heat generated by the transformer is being dissipated to the surrounding air by convection. Therefore, the phenomena will be highly affected by the velocity of the air in contact with the transformer's surfaces. In Figure 3.16 it is possible to compare the effects of the air velocity on the distribution of the temperature on the surfaces of the transformer.

From the analysis of the Figure 3.16 it is possible to conclude that the maximum surface temperatures are located on the top of the transformer. However, this surface presents itself two distinct zones, at two different temperatures.

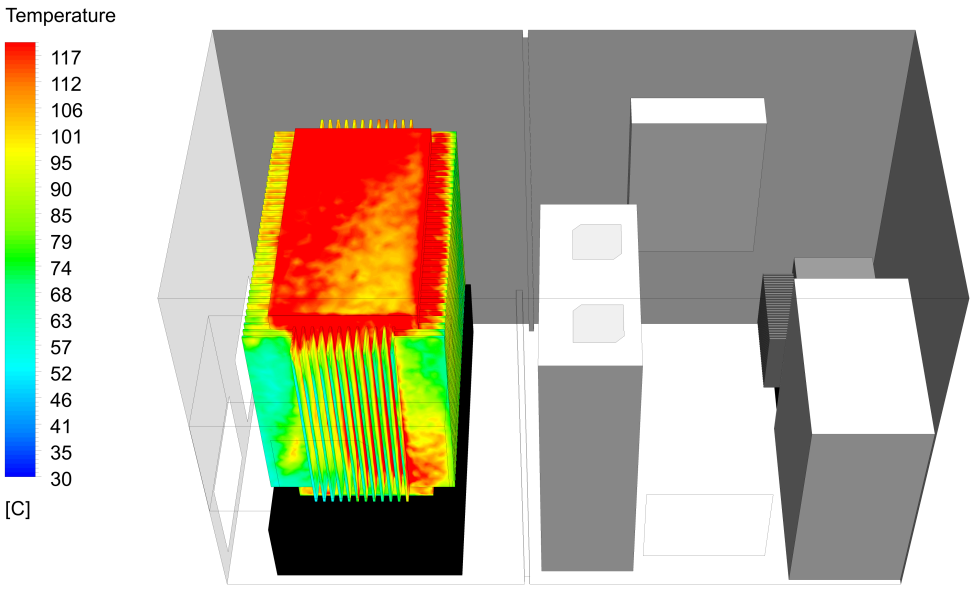

(a) View from the back wall.

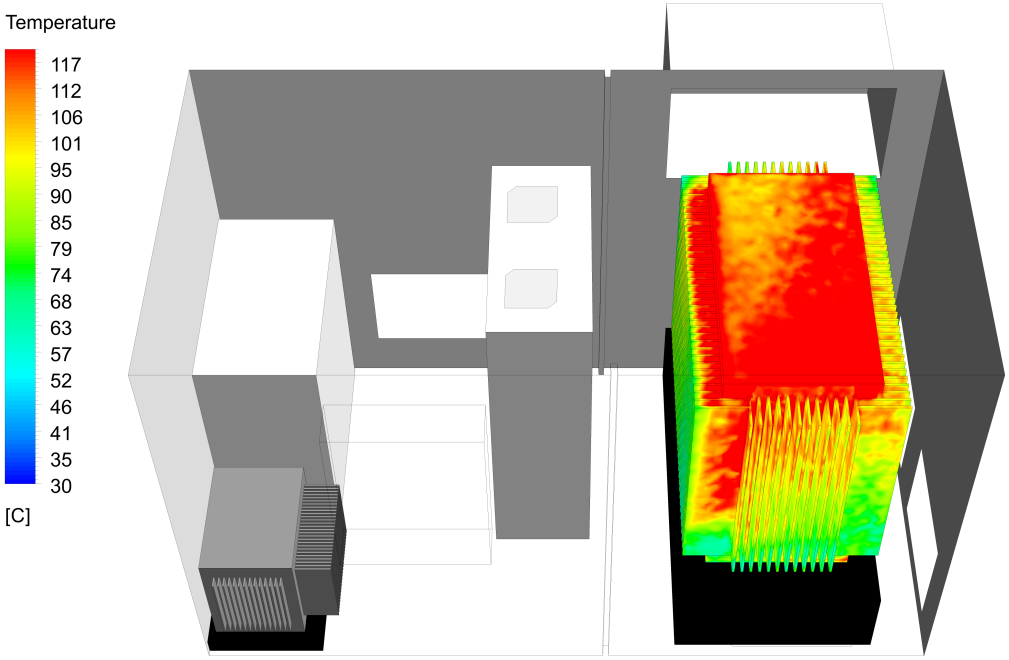

(b) View from the front wall.

Figure 3.14: Representation of the thermal distribution on the *Transformer 1750 kVA*.(1)

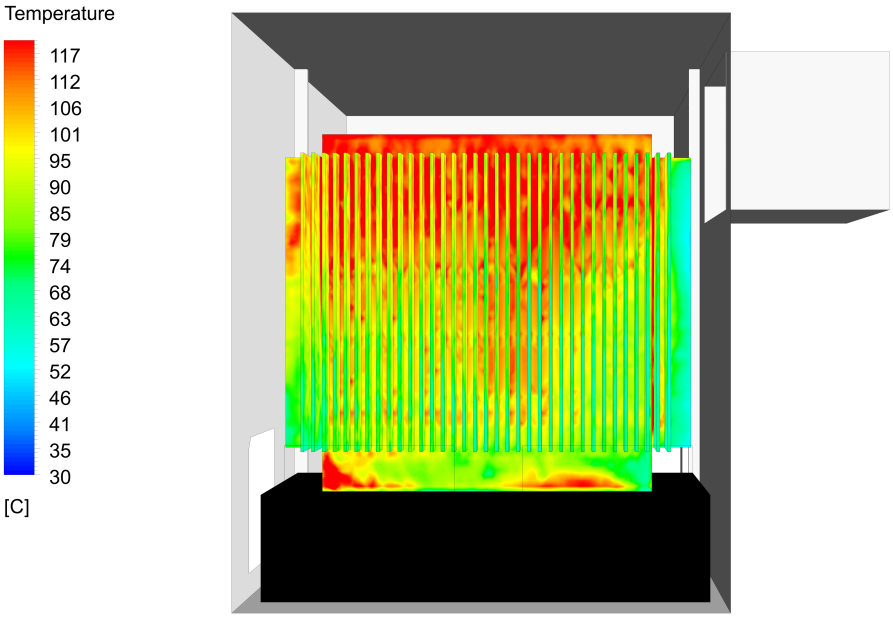

(a) View from the exterior side wall

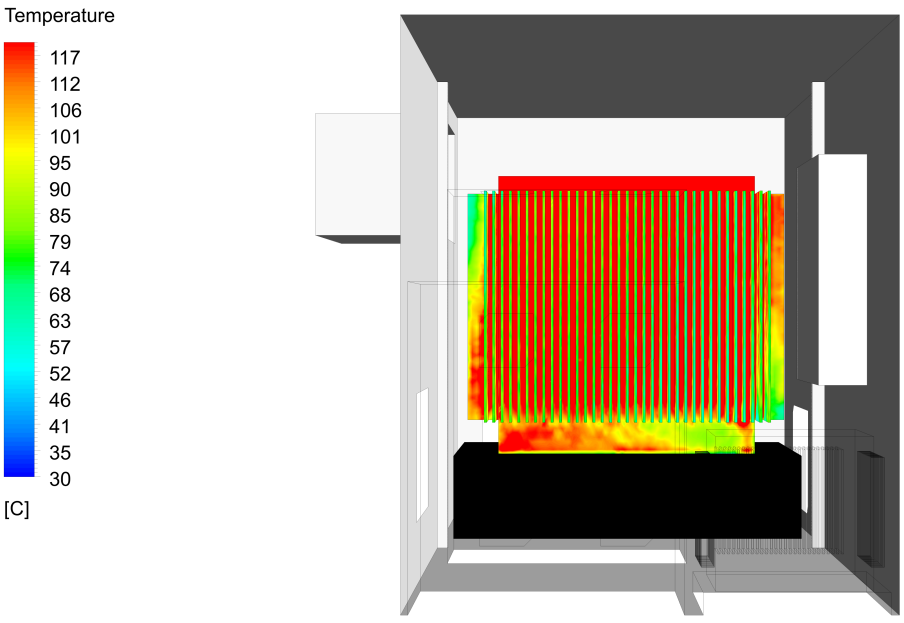

(b) View from the *Inverters' Room* side wall

Figure 3.15: Representation of the thermal distribution on the *Transformer 1750 kVA*.(2)

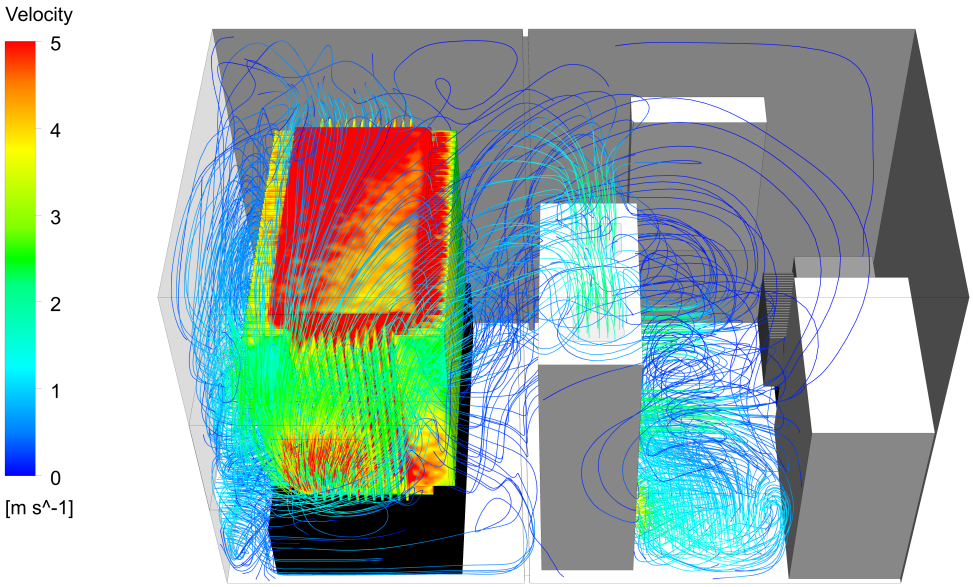

(a) View from the back wall

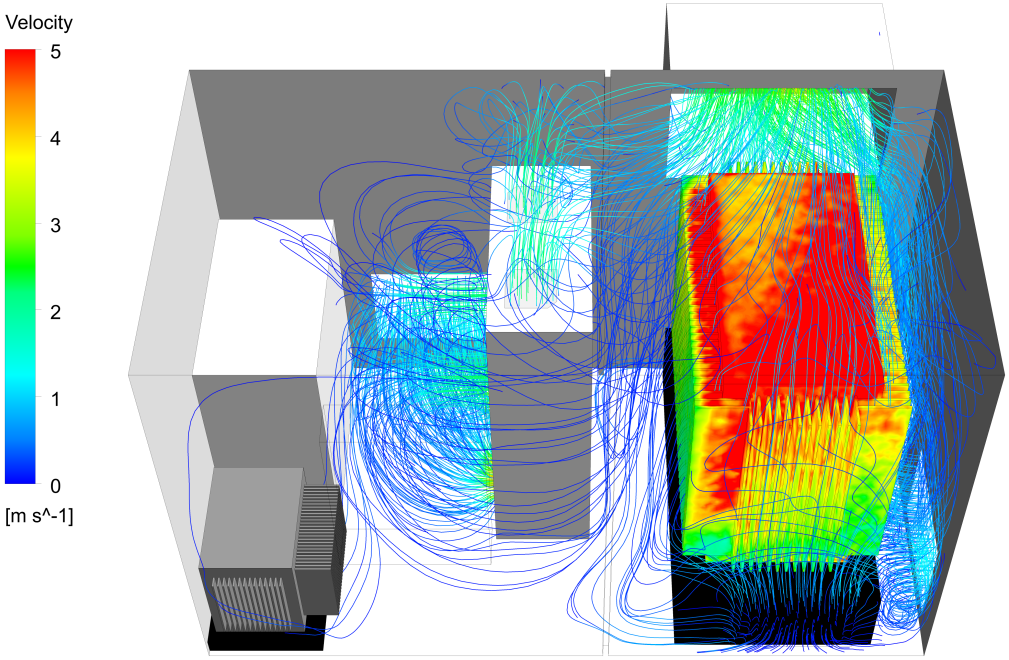

(b) View from the front wall

Figure 3.16: Representation of the thermal distribution combined with the air flow profile around the *Transformer 1750 kVA*.

This difference can be justified by the air flow profile on the surface. The air that is being released on the top of the *LV Boards* is forced out of the container by the ventilator installed on the back wall of the container, and its pathlines go through the region of lower temperature.

Unlike the air that passes through the fins, the temperature at the *LV Boards* exits is close to 35 °C, which leads to an higher efficiency of the heat transfer process.

The minimum surface temperatures are located on the bottom of the transformer. This can be explained by the proximity of the air inlets on the front and side walls. The same fact justifies the difference of temperatures between the fins located near the front and side walls and the ones located behind the *LV Boards*.

The efficiency of the heat exchanging process between the fins and the air is dependent of the difference of temperatures. As the air is passing through the fins, its temperature tends to rise, and therefore the efficiency tends to lower. Therefore, there will be a difference of temperature between the bottom and the top of the fins, as the air on the bottom is cooler than the air on the top regions.

The heat transfer coefficient is significantly dependent on the air velocity. The value presented on Table 3.7 is an average value, and therefore is not a good approximation of all the heat transfer phenomenon on the transformer. For a more detailed analysis, the transformer should be divided in smaller surface domains, and a coefficient should be calculated for each surface.

It is concluded that the amount of heat transferred to the air is consistent with the value defined previously on § 1.2. However, it must be noted that this value corresponds to the case where the transformer is operating in steady state, full load conditions, with a fixed condition of exterior air temperature of 30 °C.

In reality, these static conditions do not happen. The transformer has a dynamic behaviour. Its load cycles are dependent on external factors, such as solar radiation and electrical production on the photovoltaic cells. The external temperature of the air is also varying. A more detailed analysis of the real performance should include this fluctuations throughout the day.

3.6.4 Thermal analysis of the *Transformer 50 kVA*

As in the previous section, the numerical simulated thermal distribution profiles can be seen in Figure 3.17 and Figure 3.18. Table 3.8 present the computed values of average

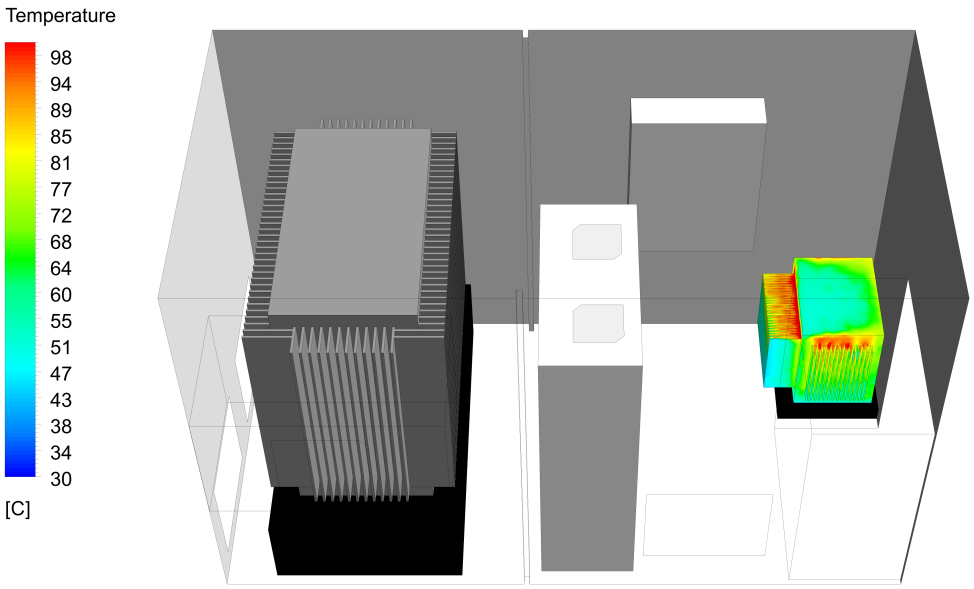

(a) View from the back wall.

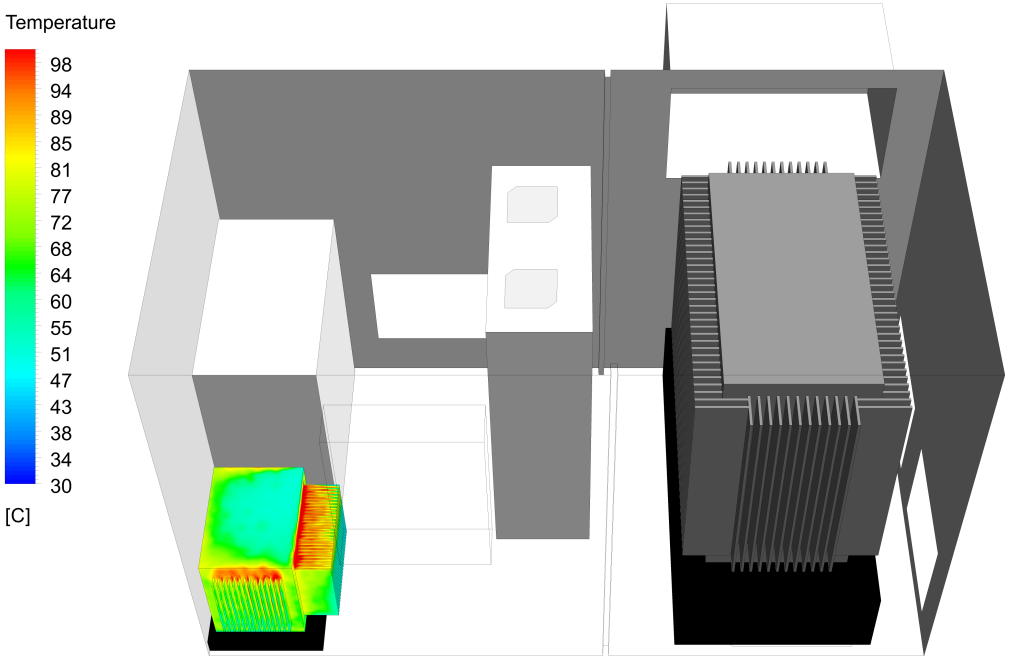

(b) View from the front wall.

Figure 3.17: Representation of the thermal distribution on the *Transformer 50 kVA*.(1)

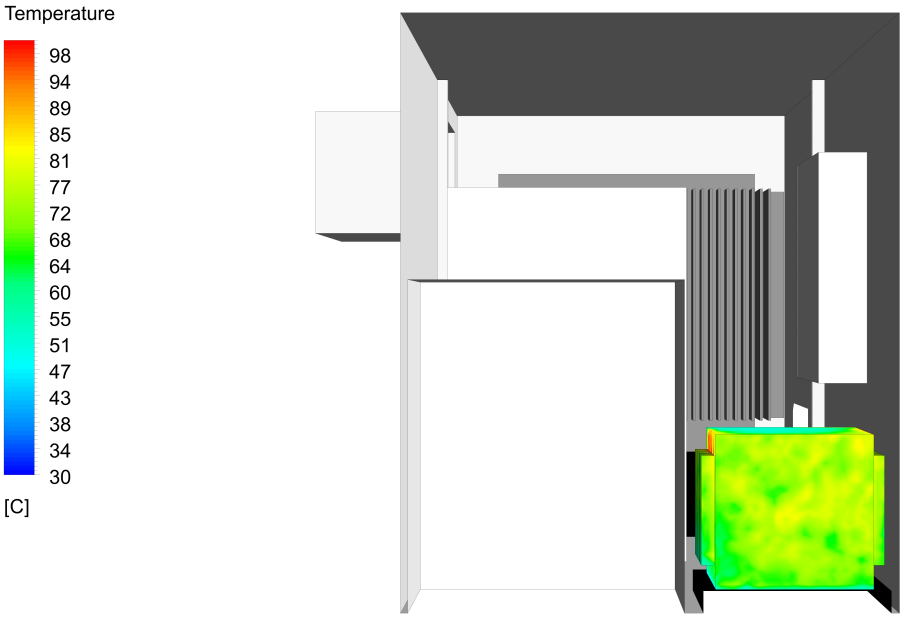

(a) View from the *Inverters' room* side wall.

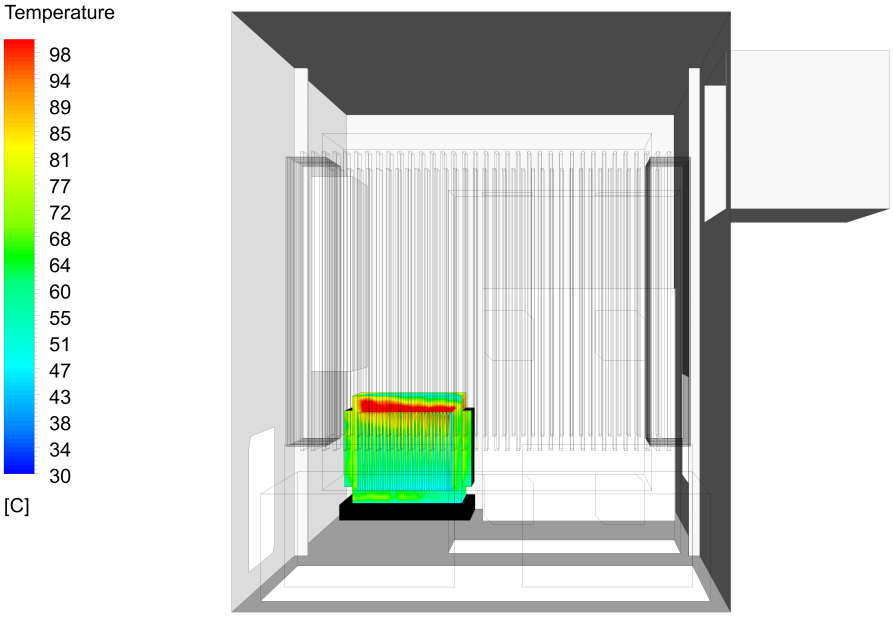

(b) View from the exterior side wall.

Figure 3.18: Representation of the thermal distribution on the *Transformer 50 kVA*.(2)

surface temperature, average heat transfer coefficient and total heal transferred on the surfaces of the transformer.

Table 3.8: Computed thermal and heat values of the *Transformer 50 kVA*.

Average surface temperature [$^{\circ}C$]	54.36
Average heat transfer coefficient [$W/m^2/^{\circ}C$]	2.81
Total heat transferred [kW]	1.29

The effects of the air velocity on the distribution of the temperature on the surfaces of the transformer are presented on Figure 3.19.

The transformers' fins present a similar thermal distribution as in the case of the thermal analysis of the *Transformer 1750 kVA*, and it is possible to assume that this behaviour is lead by the same physical heat transfer phenomena.

The value of the heat transfer coefficient is about 50% lower than the one obtained for the *Transformer 1750 kVA* case (4.58 W/m^2/°C). This is explained by the air flow on the vicinity of the transformer. The air local velocities are very low, which will therefore affect the heat transfer. In fact, due to this low velocity values, it is possible to assume that the main heat transfer phenomenon on the transformer is natural convection.

Unlike the previous, the warmest region is not on the top but on the back and side surfaces. This is justified by the fact that the transformer is positioned close to the side and front walls, and close to the *MV Board*.

The air velocity in these regions is also very low, which indicates a very low local air renewal rate. As the heat transfer process is affected by these conditions, the air will tend to warm up and the efficiency of the process will therefore be lower, leading to an increase of the surface temperatures.

The coolest regions are on the front fins and on the top surface of the transformer. The air entering the container through the back door inlet and the air expelled by the *LV Boards* internal ventilation system is partially flowing towards these regions.

Therefore, local air renewal rate will be higher than the rest of the transformer, and the heat transfer process will be more efficient, leading to a decrease of the temperature on these surfaces.

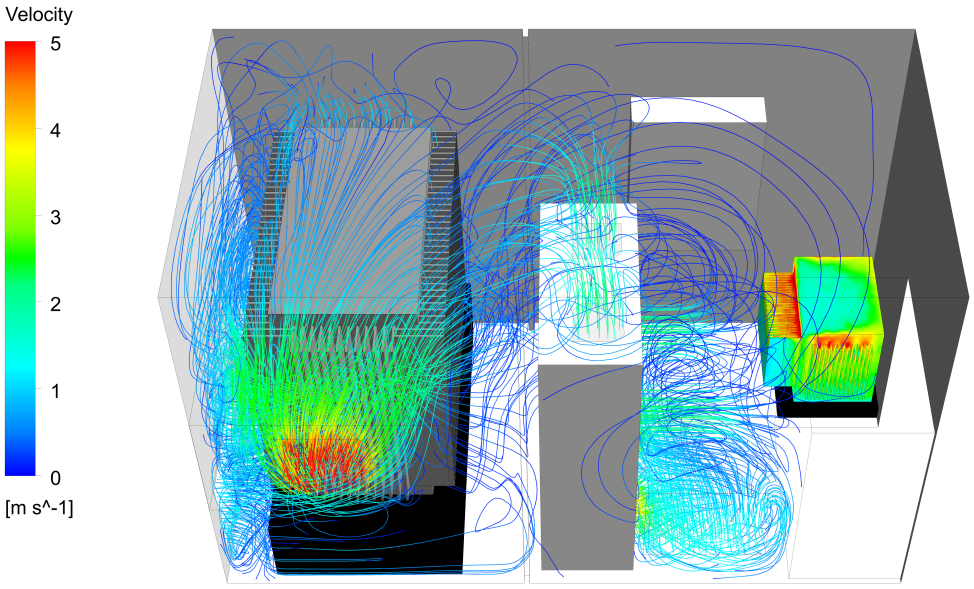

(a) View from the front wall.

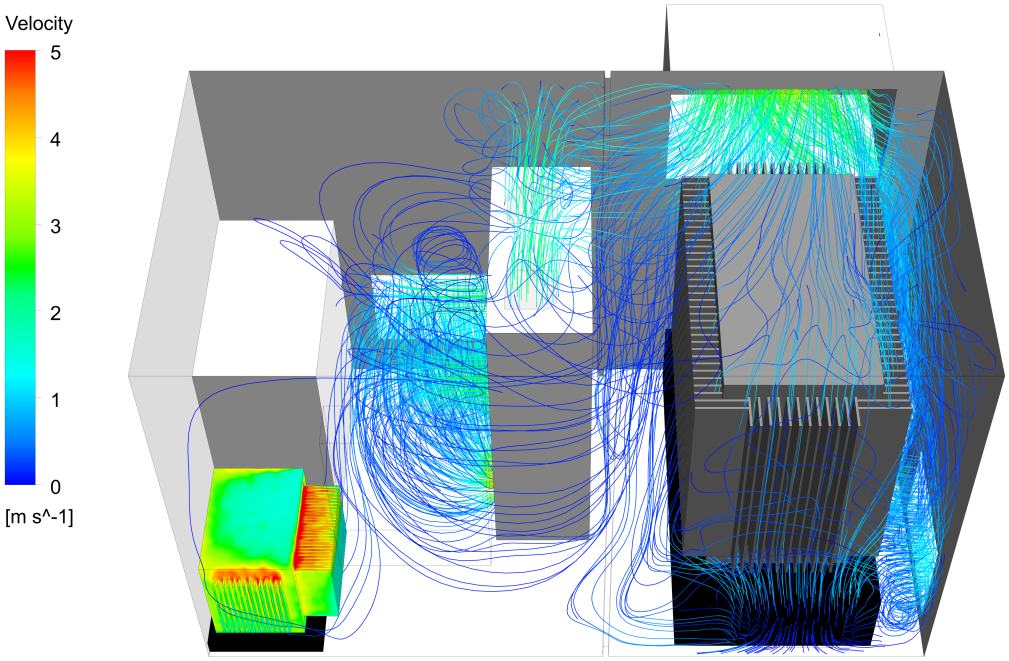

(b) View from the back wall.

Figure 3.19: Representation of the thermal distribution combined with the air flow profile around the *Transformer 50 kVA*.

3.6.5 Thermal analysis of the *LV Boards*

The *LV Boards* were modelled in a different way when compared to the equipments presented on the previous sections. They were considered as a subsystem inside the system.

Their analysis was divided in three different sections: the inlets, the outlets and the walls. The heat generated on the inside is dissipated by four ventilators, installed on the doors and top, and this is illustrated on Figure 3.20.

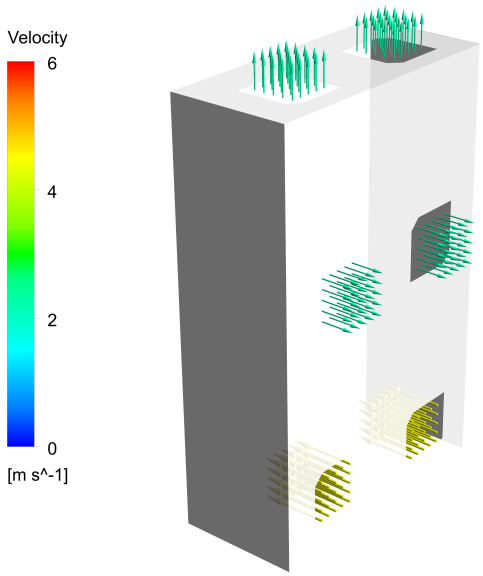

Figure 3.20: Representation of the velocities magnitude and direction on the *LV Boards*.

Table 3.9 present the computed values of volume flow rate and temperatures on both the inlets and the outlets of the boards, as well as a value of the total heat transferred to the air.

As it is mentioned before, the actual physical phenomenon that sets the air in motion is the pressure jump on the ventilators, but for simplification of the model, the velocity values on both inlets and outlets were defined (based on ventilators technical data related to volume flow rate).

This definition also simplifies the guaranty of continuity conditions on inlets and outlets too, as it is possible to observe by the equality of the volume flows. Furthermore, the value of volume flow is consistent with the one defined previously on § 1.2.

Table 3.9: Volume flow rates, temperatures and total heat transferred on the *LV Boards*.

Volume flow rate inlets [m^3/s]	-0.76
Volume flow rate outlets [m^3/s]	0.76
Temperature inlets [$^\circ C$]	32.02
Temperature outlets [$^\circ C$]	33.48
Total heat transferred [W]	1246.22

This equipment was meant to dissipate 1700 W of inside generated heat. Following the definition of the temperature of the air on the outlets and applying Eq (3.1), it is possible to observe that the ventilators do not guarantee this value of heat dissipation. The calculated heat transfer value is 1246 W, and therefore it is possible to conclude that the heat transfer process in this equipment is not accurately modelled.

$$\dot{Q} = \rho \dot{V} \cdot c_p \cdot \Delta T \tag{3.1}$$

In order to fix this, it is suggested that the temperature on the outlets (an input parameter defined in the boundary conditions) should be iteratively calculated and input on the program, until the condition of the generated heat of 1700 W is verified.

Figure 3.21 illustrates the flow profile of the air that is entering and exiting the *LV Boards*. It is possible to conclude that some of the air that is being released by the internal ventilation system is entering on the inlets of the *LV Boards*.

This happens because of the proximity between the boards' inlets and door ventilators. This will lead to a decrease of the efficiency of the heat transfer process on the inside of the equipment, and therefore contribute to the error obtained on the calculation of the amount of heat dissipated by the boards.

From the observation of the Figure 3.22, it is possible to conclude that the back surfaces of the board are warmer than the rest of the equipment, with temperatures around 40 °C. This is justified by the air velocity, flow profile and air temperature verified in that region, which was previously aborded in § 3.6.2 and § 3.6.3.

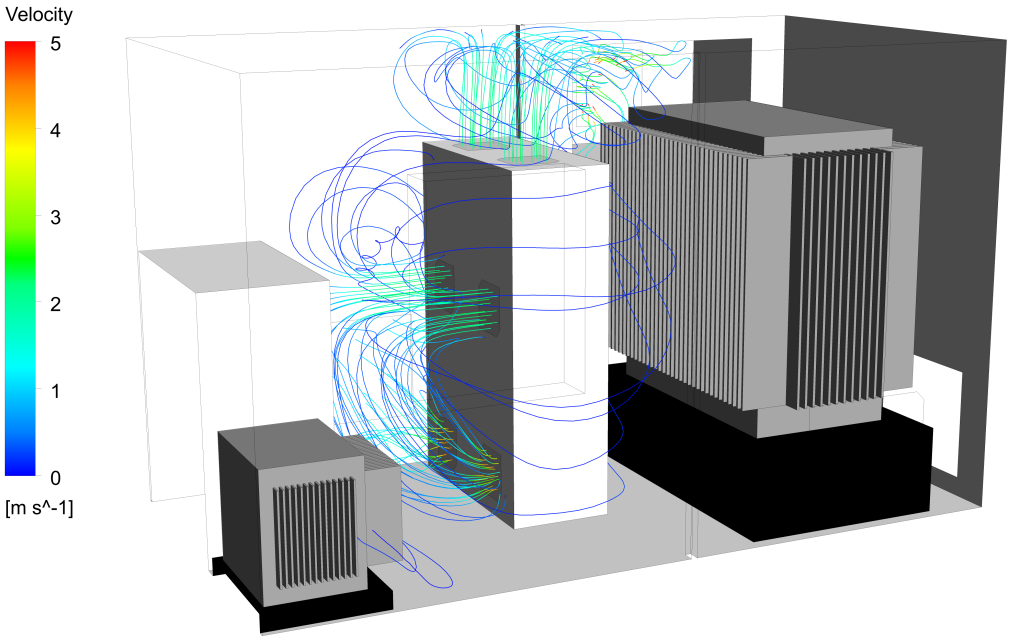

(a) View from the front wall.

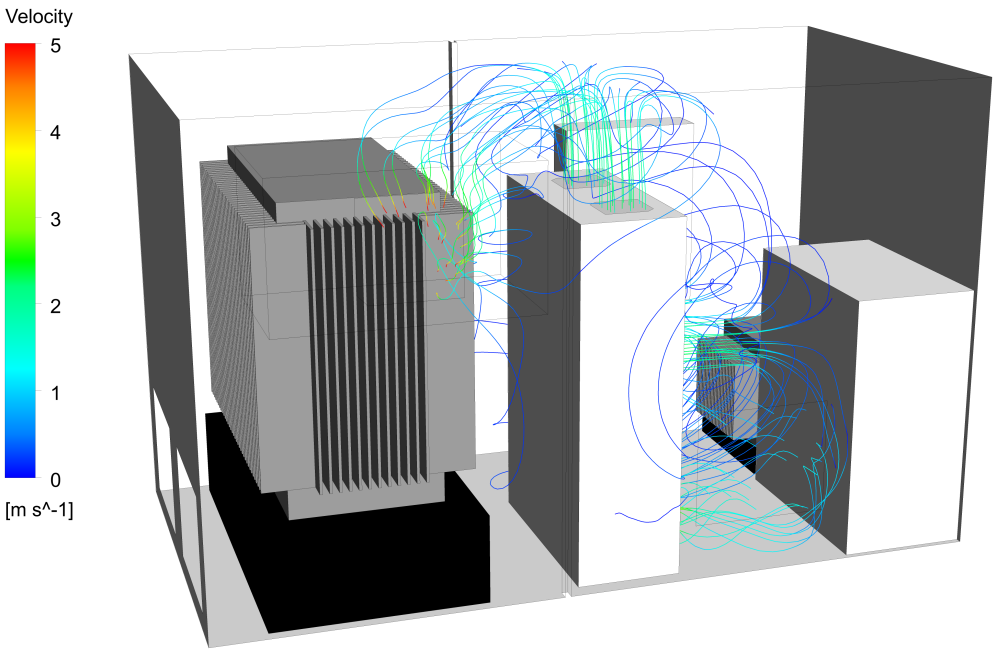

(b) View from the back wall.

Figure 3.21: Representation of the flow profile of the air entering and exiting the *LV Boards*.

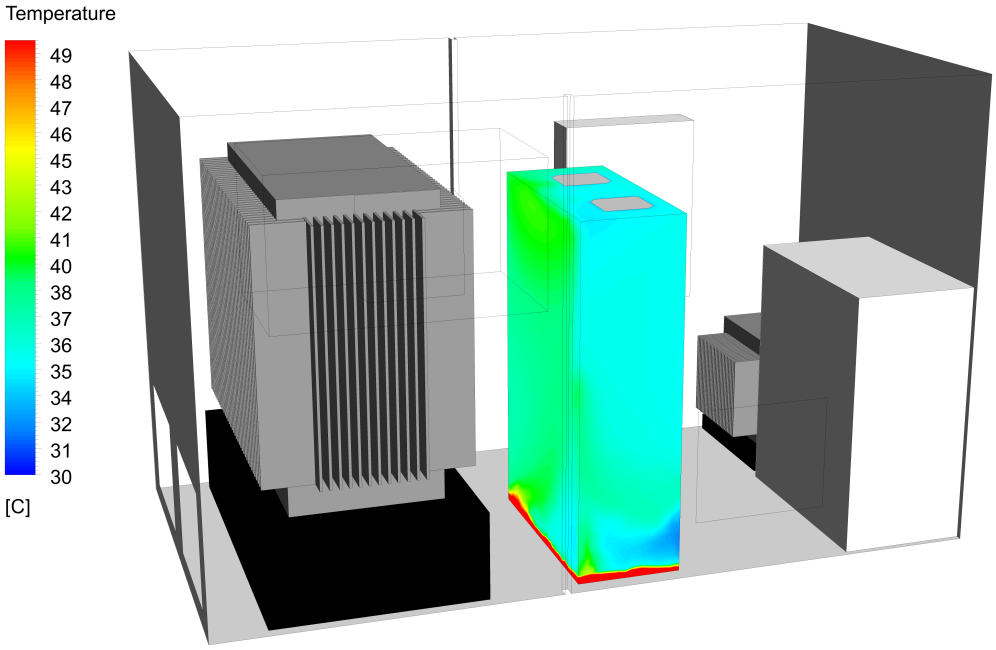

(a) View from the back wall.

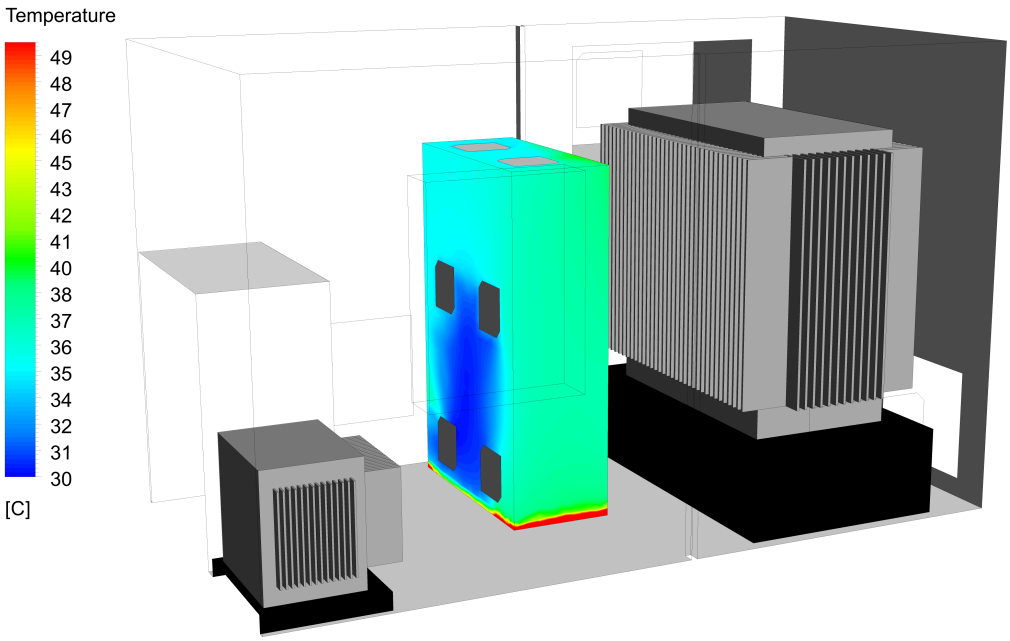

(b) View from the front wall.

Figure 3.22: Representation of the thermal distribution on the *LV Boards* walls.

On the other hand, the front surface presents the coolest region of the equipment, with temperatures between 30 °C and 35 °C. These low temperature values are influenced by the air inlet on the back door and by the internal ventilation system of the boards.

The air that is entering the container through the back door inlet goes almost directly to the boards inlet grids due to the pressure differential created by the internal ventilation system, and so it cools the regions next to these inlets.

3.6.6 Other heat sources

The heat transferred on the roof, front, back and side (exterior) walls results from the insolation effects. The container is exposed to the solar radiation during the day. Therefore, the heat gain from radiation on the exterior of the walls is going to be transferred to the interior by conduction.

In the numerical model, there are another zones besides the already mentioned that are affected by heat generation or dissipation phenomenons. In fact, only the *Monitor Box* and the *MV Board* do not present any kind of heat flux condition. In the Figure 3.23 it is possible to observe the temperature profiles of the walls, roof and floor of the *Transformers' Room*.

Table 3.10 present the computed values of heat and average surface temperature.

Table 3.10: Computed values of heat and average surface temperature on the walls, floor and roof.

	Average temperature [$^{\circ}C$]	Heat [W]
Front wall	38.59	326.62
Back wall	36.14	326.54
Inverters' room side wall	35.98	-110.25
Exterior side wall	42.26	183.75
Roof	43.58	326.55
Floor	46.65	1503.06

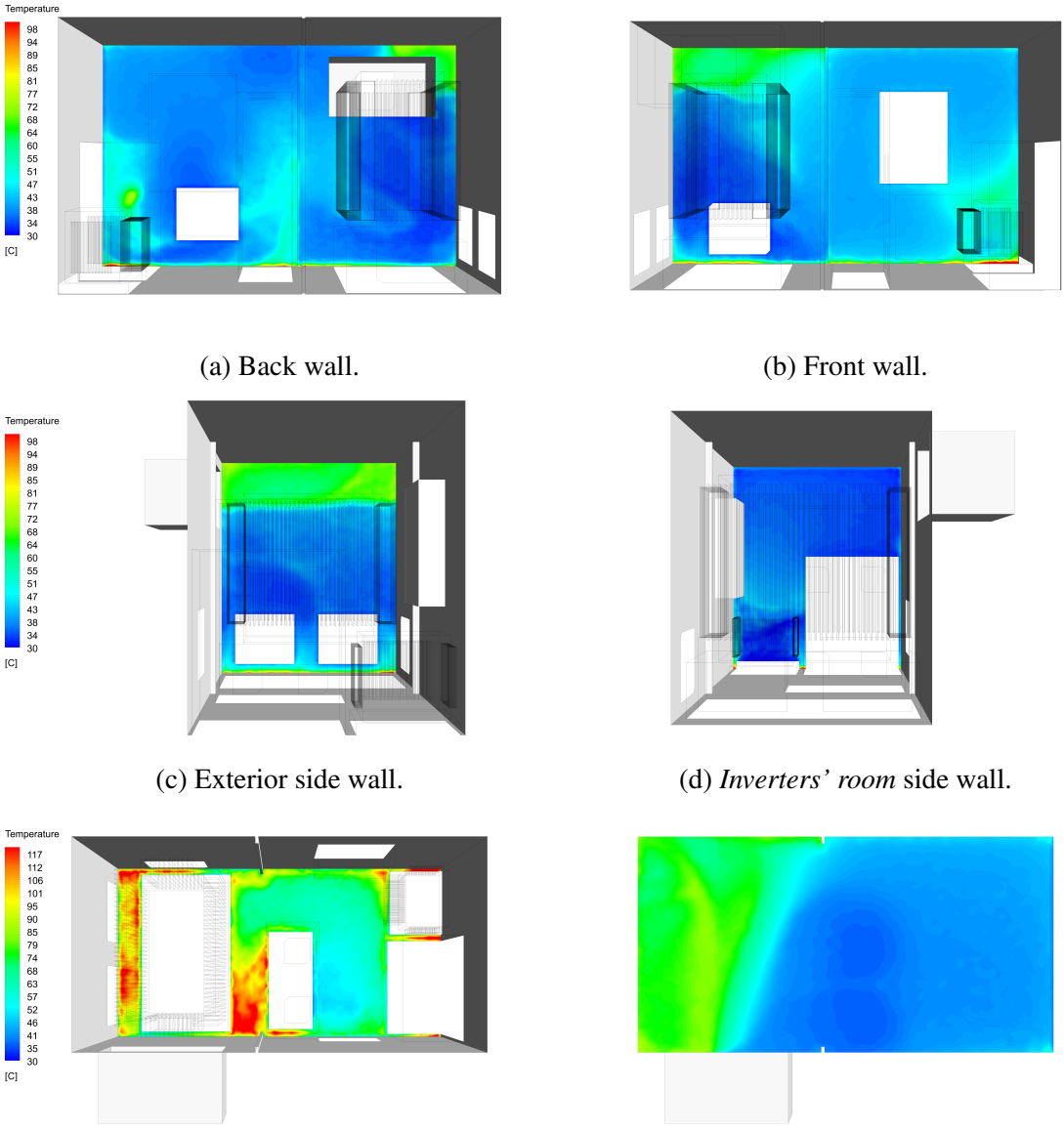

(a) Back wall.

(b) Front wall.

(c) Exterior side wall.

(d) *Inverters' room* side wall.

(e) Floor.

(f) Roof.

Figure 3.23: Representation of the air temperature distribution on the walls of the *Transformers' room*.

In the *Inverters' room* side wall, the heat flux has a negative sign. For this purpose, it must be understood that the *Transformers' room* has a physical boundary with the other container's room, where the inverters are installed.

Due to the gradient of temperature between these two rooms, an heat flux is generated and, since the temperature on the *Transformers' room* is higher, this flux is actually going out of the room, hence the negative sign.

The heat generation on the floor is a simplification of the thermal effects of the AC cables that are connecting the transformers and the inverters, located in the contiguous room. These cables are located on the floor and covered with a metal grid (technical floor). They produce heat by Joule effect. In order to simplify the model, it was considered that this heat is being generated on the whole floor surface.

If a more accurate analysis is desired, it should be taken in account the exact location of the cables. They should be represented on the model and its heat generation rate should be distinct from any possible floor heat flux.

It can be concluded that the walls' temperature profiles are deeply affected by the temperature of the air in the vicinity. The values of temperature are close to the averaged room temperature presented on Table 3.6 (38.89 °C).

3.6.7 Final heat balance

After analysing all the equipments and elements that are somehow producing or exchanging heat with the exterior, a final heat balance can be performed. This final heat balance is resumed on Table 3.11.

The difference observed on the total heat transfer values on the Table 3.11 is essentially due to the error obtained on the *LV Boards*. All the other model heat values are very close to the ones presented on the case study description (*cf.* § 1.2).

Table 3.11: Heat transfer balance inside the *Transformers' room*.

	Table 1.1 values [W]	Model values [W]
Transformer 1750 kVA	20900.00	20899.88
Transformer 50 kVA	1290.00	1290.00
LV Boards	1700.00	1246.22
Front wall	326.55	326.62
Back wall	326.55	326.54
Inverters' room side wall	-110.25	-110.25
Exterior side wall	183.75	183.75
Roof	326.55	326.55
Floor	1503.07	1503.06
Total	26446.22	25992.37
Error [%]		1.72

Chapter 4

Closure

4.1 Conclusions

In this work, a numerical simulation was used to obtain the air flow profile and the temperature distribution inside the *Transformers' room*.

From the analysis of the air flow patterns it was concluded that the air entering through the front door and side wall inlets tended to flow around the wall side of the transformer and go directly to the ventilator. The major quantity of the air entering through the back door inlet is flowing towards the *LV Boards* inlets.

The *Transformer 1750 kVA* was blocking the entrance of air from the inlets on the side wall and front door. The volume flow rates on these faces were substantially lower than the one on the back door inlet, which was not blocked by any equipment.

The short distance between the transformer and the inlets affect not only the pattern of the fluid flow but also the air velocity in those regions, which influences the convection process.

The hottest region of the model were the top surface of the *Transformer 1750 kVA*, with temperatures around 120 °C. This was the equipment that influenced the most the air temperature distribution.

The coolest regions of the model were adjacent to the air inlets on the side wall and on the front and back doors, where the temperature of the air was still not affected by the heat sources inside the container, and therefore it was almost the same as the temperature on the outside (30 °C).

The average interior air temperature was 39 °C.

It was observed that the air next to the *Transformer 1750 kVA* fins was the same as the initial entrance temperature. Due to the proximity of the inlets and the tight space between the transformer and the walls, the air velocity was higher in these regions, which meant that the local air renewal rate was higher than in the rest of the room. Its heat generation influenced the air temperature in the space between the transformer and the *LV Boards*. The local air renewal rate was low and the heat transferred on the transformer's fins from that side tended to increase the local air temperature (42 °C).

The heat generation of the *Transformer 50 kVA*, combined with the low values of the local velocity, originated a region of hot air with temperatures around 45 °C, on the corner where the transformer is located.

The heat transfer process in the *LV Boards* was not accurately modelled, as the equipment was meant to dissipate 1700 W and the calculated heat transfer value was 1246 W. In order to fix this, it was suggested an alteration of the temperature boundary conditions on the outlets. Plus, some of the air that was being released in *LV Boards* outlets was recirculating and is entering on its inlets. This happened because of the proximity between the boards' inlets and door ventilators, leading to a decrease of the efficiency of the heat transfer process on the inside of the equipment.

It was possible to conclude that the walls' temperature profiles were deeply affected by the temperature of the air in their vicinities.

As a final note, it must be reminded that the model presented in this work is still lacking validation. Possible differences between the real case scenario and the numerical model results can be caused by inaccurate values of heat flux presented on the heat quantification study presented on § 1.2.1.1.

4.2 Topics for future research

The following topics are proposals for future improvements on the work presented on this thesis, which would certainly increase the quality of the numerical model and lead to more accurate results.

First of all, it is suggested evaluate the sensibility of the results of the study to different turbulence models.

It is suggested to change the boundary conditions of all the ventilators, from the current imposition of velocity to the imposition of the ventilator pressure jump, and note the main differences between the new and the current model.

In the real case situation, the entrance grids have air filters installed. These filters introduce a resistance coefficient on the air flow that is not considered in this work. A more accurate analysis should account these effects.

The exterior air temperature considered is a fixed value. The transformers operating conditions are also considered to be fixed, in steady state, full load regime. In reality, these static conditions do not happen. The transformer has a dynamic behaviour. Its load cycles are dependent on external factors, such as solar radiation and electrical production on the photovoltaic cells. The external temperature of the air is also varying. A more detailed analysis of the real performance should include this fluctuations throughout the day.

The radiation heat transfer between the equipments and the walls is not accounted on this model, and can be implemented on further improvements. The effects of the insolation can also be input, considering its fluctuation throughout the day too.

The exact location of the cables should be known in order to correctly input its heat generation value on its precise spacial location.

In order to effectively validate the model, in-sight measurements should be performed and compared with the results of the numerical simulations.

Bibliography

ANSYS Documentation (2013), *ANSYS Documentation*, Release 15.0 edn, ANSYS, Inc., Southpointe, 275 Technology Drive, Canonsburg, Pennsylvania.

Barth, T. J. and Jespersen, D. (1989), The Design and Application of Upwind Schemes on Unstructured Meshes, Technical Report AIAA-89-0366, AIAA 27th Aerospace Sciences Meeting, Reno, Nevada, USA.

Batchelor, G. K. (1967), *An Introduction to Fluid Dynamics*, Cambridge University Press.

Choi, H. and Moin, P. (2012), 'Grid-Point Requirements for Large Eddy Simulation: Chapman's Estimates Revisited', *Physics of Fluids* **24(1)**, 011–702.

Coleman, H. W. and Stern, F. (1997), 'Uncertainties and CFD Code Validation', *ASME Journal of Fluids Engineering* **199**, 795–803.

El Wakil, N., Chereches, N. C. and Padet, J. (2006), 'Numerical Study of Heat Transfer and Fluid Flow in a Power Transformer', *International Journal of Thermal Sciences* **45**, 615–626.

Ferziger, J. H. and Perić, M. (2002), *Computational Methods for Fluid Dynamics*, 3rd revised edn, Springer.

Issa, R. I. (1986), 'Solution of the Implicitly Discretised Fluid Flow Equations by Operator-Splitting', *Journal of Computational Physics* **62**, 40–65.

Kim, S. E., Choudhury, D. and Patel, B. (1997), Computations of Complex Turbulent Flows Using the Commercial Code ANSYS Fluent, *in* 'ICASE/LaRC/AFOSR Symposium on Modeling Complex Turbulent Flows', Hampton, Virginia, USA.

Kline, S. J., Cantwell, B. J. and Lilley, G. (1980), The 1980-81 AFOSR-HTTM-Stanford Conference on Complex Turbulent Flows: Comparison of Computational and Experiment, Technical report, Thermosciences Division, Mechanical Engineering Department, Stanford University, Stanford, California, USA.

Launder, B. E., Reece, G. C. and Rodi, W. (1975), 'Progress in the Development of a Reynolds-Stress Turbulence Closure', *Journal of Fluid Mechanics* **68**, 537–566.

Launder, B. E. and Sharma, B. I. (1974), 'Aplication of the Energy-Dissipation Model of Turbulence to the Calculation of Flow near a Spinning Disc', *Letters in Heat and Mass Tranfer* **1**, 131–138.

Launder, B. E. and Spalding, D. B. (1972), *Lectures in Mathematical Models of Turbulence*, Academic Press, London, England.

Lesieur, M. and Métais, O. (1996), 'New Trends in Large-Eddy Simulations of Turbulence', *Annual Review of Fluid Mechanics* **28**, 45–82.

Moin, P. (1997), 'Progress in Large-Eddy Simulation of Turbulent Flows', *AIAA Journal* **97**, 07–49.

Moin, P. and Mahesh, K. (1998), 'DIRECT NUMERICAL SIMULATION: A tool in Turbulence Research', *Annual Review of Fluid Mechanics* **30**, 539–578.

Munson, B. R., Young, D. F., Okiishi, T. H. and Huebsch, W. W. (2009), *Fundamentals of Fluid Mechanics*, Wiley.

Oberkampf, W. L. and Trucano, T. G. (2002), 'Verification and Validation in Computational Fluid Dynamics', *Progress in Aerospace Sciences* **38**, 209–272.

Patankar, S. V. (1980), *Numerical Heat Transfer and Fluid Flow*, Hemisphere.

Patankar, S. V. and Spalding, D. B. (1972), 'A Calculation Procedure for Heat, Mass and Momentum Transfer in Three-dimensional Parabolic Flows', *International Journal of Heat and Mass Transfer* **15**, 1787.

Pope, S. B. (2000), *Turbulent Flows*, Cambridge University Press.

Ramos, J. C., Beiza, M., Gastelurrutia, J., Rivas, A., Antón, R., Larraona, G. S. and de Miguel, I. (2013), 'Numerical Modelling of the Natural Ventilation of Underground Transformer Substations', *Applied Thermal Engineering* **51**, 852–863.

Reynolds, O. (1895), 'On the Dynamical Theory of Incompressible Viscous Fluids and the Determination of the Criterion', *Philosophical Transactions of the Royal Society of London* **186**, 123–164.

Rhie, C. M. and Chow, W. L. (1983), 'Numerical Study of the Turbulent Flow Past an Airfoil with Trailing Edge Separation', *AIAA Journal* **21(11)**, 1525–1532.

Roache, P. (1994), 'Perspective: A Method For Uniform Reporting Of Grid Refinement Studies', *ASME Journal of Fluids Engineering* **116**, 405–413.

Roache, P. (1998), *Verification and Validation of Computational Science and Engineering*, Hermosa Publishers, Albuquerque, New Mexico, USA.

Shih, T. H., Liou, W. W., Shabbir, A., Yang, Z. and Zhu, J. (1995), 'A New k-ε Eddy-Viscosity Model for High Reynolds Number Turbulent Flows - Model Development and Validation', *Computers Fluids* **24(3)**, 227–238.

Silva Lopes, A. (2000), Simulação das Grandes Escalas da Turbulência em Geometrias Complexas, PhD thesis, Faculdade de Engenharia da Universidade do Porto.

Smagorinsky, J. (1963), 'General Circulation Experiments with the Primitive Equations', *Monthly Weather Review* **91(3)**, 99–164.

Speziale, C. G. (1991), 'Analytical methods for the development of Reynolds-stress closures in turbulence', *Annual Review of Fluid Mechanics* **23**, 107–157.

Tsili, M. A., Amoiralis, E. I., Kladas, A. G. and Souflaris, A. T. (2012), 'Power Transformer Thermal Analysis by Using an Advanced Coupled 3D Heat Transfer and Fluid Flow FEM Model', *International Journal of Thermal Sciences* **53**, 188–201.

Vandoormaal, J. P. and Raithby, G. D. (1984), 'Enhancements of the SIMPLE Method for Predicting Incompressible Fluid Flows', *Numeric Heat Transfer* **7**, 147–163.

Veiga Rodrigues, C. A. (2013), Computer Modelling of Atmospheric Flows in Wind Energy Applications, PhD thesis, Faculdade de Engenharia da Universidade do Porto.

Versteeg, H. K. and Malalasekera, W. (2007), *An Introduction to Computational Fluid Dynamics*, second edition edn, Pearson Education Limited.